159
120

MODELING AND STABILITY INVESTIGATION OF A GLULAM DOME

by

Chen-Hung Wu

Thesis submitted to the Faculty of the

Virginia Polytechnic Institute and State University

in partial fulfillment of the requirements for the degree of

Master of Science

in

Civil Engineering

APPROVED:

S. M. Holzer, Chairman

J. R. Loferski

D. A. Garst

March 1991

Blacksburg, Virginia

MODELING AND STABILITY INVESTIGATION OF A GLULAM DOME

by

Chen-Hung Wu

S. M. Holzer, Chairman

Civil Engineering

(ABSTRACT)

In order to predict the ultimate load capacity and failure modes of a glued-laminated timer dome, two dome models are analyzed by two finite element methods. I-DEAS is utilized to generate shell elements and to compute nodal forces for the dome model. Wind load requirements are studied, and the effect of wind loads is investigated.

At first, linear and nonlinear analyses of a space frame are carried out for four load combinations of dead load and snow load. The results are applied as a basis for the modeling of flexible joints and bracings.

Then, the 3-D, 3-noded, curved, isoparametric beam element in the first model is replaced by a 3-D, 2-noded, straight beam element for the second model. Purlins consist of truss elements. Flexible joints are modeled by adding connector elements to the ends of each beam. A bracing of truss element is applied to simulate the contribution of the decking. The dome is analyzed for two load conditions. The buckling pressures, buckling modes and the material behavior prior to buckling are examined.

Finally, conclusions are made and several topics are recommended for future studies.

Acknowledgements

I am deeply grateful to Dr. S. M. Holzer for his teaching, patience and encouragement throughout my study.

I feel very much indebeted to Professor D. A. Garst for his generosity and participating in the committee. I also wish to express my sincere appreciation to Dr. J. R. Loferski for his helpful suggestion and reviewing the thesis.

Special thanks go to J. Tissaoui for providing guidence to use I-DEAS.

Finally, I would like to dedicate this thesis to my family for their understanding and support.

Table of Contents

INTRODUCTION **1**

1.1 General 1

1.2 Background 3

METHODS OF STABILITY ANALYSIS **6**

2.1 Nonlinear Analysis 7

2.2 Combined Analysis 7

2.3 Comparison 9

2.4 Nonlinear Analysis With ABAQUS 9

MODEL AND LOAD **12**

3.1 Selection of Elements 13

3.2 Material Properties 14

3.3 Boundary Conditions 15

3.4 Design Loads 15

3.4.1 Dead Load 15

3.4.2 Live Load 16

3.4.3 Wind Load 16
3.5 Stability Study Modeling 19
3.6 Load Generation 20

ANALYSIS OF B32 MODEL 26
4.1 Linear Analysis 27
4.2 Nonlinear Analysis 27
4.3 Maximum Stress 28
4.4 Discussion 29

EVALUATION OF B33 MODEL 36
5.1 Linear Analysis 36
5.2 Nonlinear Analysis 38
5.3 Wind Load Effect 39

STABILITY INVESTIGATION 42
6.1 Models Without Bracing 43
6.2 Models With Bracing 45
6.3 Discussion 46
6.3.1 Uniform Snow Load 46
6.3.2 Half Snow Load 47

CONCLUSIONS AND RECOMMENDATIONS 64
7.1 Conclusions 65
7.2 Recommendations 67

BIBLIOGRAPHY 68

Listing of Fortran Program 70

Comparison of Element Stresses for Three B33 Models 73

Vita 75

List of Illustrations

Figure 2.1. Buckling load prediction. 11

Figure 3.1. Triax dome model 21

Figure 3.2. (a) Dimensions of the members of the dome model; (b) Tributory areas of one panel. 22

Figure 3.3. ECCS wind pressure coefficients for domes. 23

Figure 3.4. (a) Wind pressure distribution for the dome model; (b) Shell elements of one sector. 24

Figure 3.5. (a) One sector of the B33 model; (b) B33 elements of one sector for stress checking. 25

Figure 4.1. (a) B32 elements of one sector for stress checking; (b) Element cross section for stress checking. 30

Figure 4.2. Critical load prediction curves for (a) snow over the entire dome and (b) snow over inner half of the dome. 31

Figure 4.3. Critical load prediction curves for (a) snow over outer half of the dome and (b) snow over half the dome. 32

Figure 4.4. Equilibrium paths for (a) snow over the entire dome and (b) snow over half the dome 33

Figure 4.5. Buckling modes for (a) snow over the entire dome and (b) snow over half the dome. 34

Figure 6.1. Critical load prediction curves for models without bracing and with (a)100%; (b)25% joint stiffnesses for uniform snow load. 49

Figure 6.2. Critical load prediction curves for models without bracing and with (a)100%; (b)25% joint stiffnesses for half snow load. 50

Figure 6.3. Buckling mode of the models with 100% and 25% joint stiffnesses for snow over the entire dome. 51

Figure 6.4. Buckling mode of the models with 100% and 25% joint stiffnesses for snow over half the dome. 52

Figure 6.5. Equilibrium paths of the models with (a)rigid joints without bracing;(b)25% joint stiffness with bracing for half snow load. 53

Figure 6.6. (a) Critical load parameter versus joint stiffness; (b) Bracing area versus critical load parameter. 54

Figure 6.7. Critical load prediction curves of the models with bracing and with (a)100%; (b)25% joint stiffnesses for uniform snow load. 55

Figure 6.8. Critical load prediction curves of the models with bracing and with (a)100%; (b)25% joint stiffnesses for half snow load. 56

Figure 6.9. Buckling mode of the models with bracing (A = 0.1) and with 100% or 25% joint stiffness for snow over the entire dome. 57

Figure 6.10. Buckling mode of the model with bracing (A = 0.45) and rigid joints for snow over the entire dome. 58

Figure 6.11. Buckling mode of the models with bracing (A = 0.3) and with 100% or 25% joint stiffness for snow over half the dome. 59

Figure 6.12. Equilibrium paths of the models with rigid joints and with bracings (a) A = 0.10; (b) A = 0.45 for snow over the entire dome. 60

List of Tables

Table 4.1. (a) Buckling load prediction for uniform snow load; (b) Maximum stresses just before buckling for B32 models. 35

Table 5.1. Maximum stresses of linear analyses. 41

Table 6.1. Maximum stresses of linear analyses for (a) snow over the entire dome and (b) snow over half the dome. 61

Table 6.2. Critical load parameters for (a) snow over the entire dome and (b) snow over half the dome. 62

Table 6.3. Maximum stresses just before buckling for (a) snow over the entire dome and (b) snow over half the dome. 63

Chapter 1

INTRODUCTION

1.1 General

Various types of lattice domes have been constructed during the past two centuries (Task Committee on Latticed Structures, 1976). Most of these domes are constructed of light-weight materials like steel and aluminum. The use of glued-laminated (glulam) members was introduced recently. Glulam domes, such as Triax (Neal, 1973) and Varax (Eshelby and Evans, 1988) domes, have been entered in the market. They possess lower construction cost, better energy conservation and offer superior accoustic response and beauty (Davalos, 1989). The largest timber dome built in the world is the Tacoma Dome which has a span of 530 ft. and a rise of 110 ft. (Pacific Builder and engineeer, 1983).

Although these glulam domes appear to have been well designed and constructed, their structural response and safety are still not fully understood. A method to predict their ultimate load capacities

and failure modes has to be established. Holzer and Loferski (1987) provide the most valuable information for the development of a finite element method.

A triax dome built in Raleigh, N.C. was selected as the dome model. Two finite element methods are used in the analyses: A nonlinear analysis that traces the equilibrium path through the first critical point and a combined nonlinear/linear eigenvalue method that provides estimates of the buckling load.

The finite element software ABAQUS (version 4.8, 1990) was chosen as the tool of analysis to evaluate the response of the dome. In order to evaluate the effect of wind loads on domes, a study of several available codes and papers was made to establish the pressure distribution and perform analysis.

Two different models are used in the analyses. The first model is a space frame composed of 3-noded, curved, isoparametric beam elements and rigid joints. The dome is analyzed for four load combinations of dead load and snow load.

The second model uses 2-noded, straight beam elements for both beams and purlins. Purlins are modeled as truss elements to reduce the degrees of freedom at two ends and to represent the pinned-connection of the beam-purlin joints. Flexible joints are modeled by modifying the moments of inertia of the connector elements. The contribution of the decking is simulated by the bracing to provide lateral support to the beams. Two load conditions of uniform snow load and half snow load are applied in the analyses. The effect of wind loads is evaluated by using the second model with rigid joints for two load conditions of dead load, wind load, and with or without half snow load.

Equilibrium paths and buckling modes are plotted for some selected models. The extreme stresses are checked against the proportional limit and the ultimate stresses from the Wood Handbook

(1987). Thus, the status of the glulam beams prior to buckling can be ascertained. The effects of the joint stiffness and the bracing are discussed.

The thesis presents part of the work to gain insight into the behavior of spatial wood structures and to develop models that are sufficiently simple to use in engineering practice and yet reflect the dominant characteristics of these structures (Holzer, Wu, and Tissaoui, 1991). The objects in this study are:

1. To investigate a 3-D model in which a 2-noded, straight beam element is used for beams.

2. To compute and study the effect of wind pressures.

3. To explore the effect of the flexible joints.

4. To simulate the contribution of the decking.

5. To study the combined effects of the joint stiffness and the bracing on the stability of the dome.

1.2 Background

In the past, the stability of lattice or reticulated structures was analyzed by using continuous mathematical models. Instability is detected by using the buckling load of an equivalent continuous shell obtained by the conventional shell theory. The buckling state based on this theory is determined by linear membrane theory (Task Committee on Latticed Structures, 1976).

Generally, the prebuckling behavior of lattice domes exhibits large joint displacements and large member rotations. Nonlinear effects must be included to accurately predict the response of these

structures. However, the criteria for introducing shell buckling formulas into the nonlinear analysis of reticulated structures were not established (Rothert et al., 1981).

With the fast development of large electronic computing facilities, it seems expedient to resort to a discrete element analysis. Rothert et al. (1981) developed a geometrically nonlinear displacement method and made a comparative study on computational efforts and effectiveness for four methods by evaluating numerical results. They concluded that the Newton-Raphson method combined with the extrapolation of the relative determinant is the most economical means to determine the limit point with sufficient accuracy. If the loading path beyond the limit point is of interest, they recommended to use methods like those of Menzel and Schwetlick, Riks, and Wempner. A complete review of the finite element methods that are used to investigate the stability of spatial structures has been done by Holzer, Davalos, and Huang (1989).

The present nonlinear analysis capability includes material nonlinearity, geometric nonlinearity and boundary nonlinearity (ABAQUS). There is a complete introduction and formulation of finite elements for linear and nonlinear analyses by Bathe (1982). His guidence is very helpful for us in selecting the appropriate elements for the dome model.

Several papers reported that elastic instability dominates the failure of single-layer metal domes (Tsuboi, 1984; Holzer and Loferski, 1987). The snap-through load of reticulated shells is sensitive to asymmetries of loadings and stiffness (Rothert et al., 1981). The buckling load of a reticulated single-layer shell is more significantly affected by the rise-to-span ratio for the pin-connected joints than for rigidly-connected joints (Hangai and Ohya, 1988). However, the material property of glulam members differs from that of steel considerably. The value of the shear modulus is relatively low. Nevertheless, the assumption of elastic instability is adopted in this study.

Wind load and snow load are two most important design loads for lattice domes (Baker, 1984). Although most U.S. codes specify design requirements for the two loads, they do not provide dis-

tributions and intensities of wind loads for domes. Generally, a wind tunnel test is recommended to determine the distribution of wind pressures (ANSI, 1982).

A detailed comparision of all the available codes concerning wind loading by Baker (1984), indicates that there are significant differences in the practice adopted by various countries. He states that the limited information contained in the Wind Loading Handbook (Newberry and Eaton, 1974), which is based mainly on the work of Maher (1966), is the best available. The pressure distribution suggested by the European Convention for Constructional Steelwork has broad agreement with that provided by the Wind loading Handbook.

The wind pressure coefficients for domes contained in the ECCS are clearly defined and easy to apply. They are combined with the basic wind speed and wind pressure equations from ANSI A58.1-1982 to calculate wind load on the dome model.

Chapter 2

METHODS OF STABILITY ANALYSIS

A nonlinear analysis and a combined nonlinear/linear eigenvalue analysis are used to investigate the stability of the glulam dome. Two methods of nonlinear analysis are presented in Section 2.1. An eigenvalue buckling prediction is discussed in Section 2.2.

Proportional loading is applied throughout the nonlinear analyses. For a dome under two independent load conditions, a dead load and a live load, the applied pressure p is expressed as

$$p = p_D + \lambda p_L$$

where p_D is the dead load, p_L is the live load, and λ is the proportionality factor of the live load.

The relations between the nonlinear analysis and the combined analysis are discussed in Section 2.3. Some general guidelines for conducting nonlinear analyses with ABAQUS are presented in Section 2.4.

2.1 Nonlinear Analysis

Two incremental iterative procedures, the Newton/Raphson method and the modified Riks/Wempner method, are applied to trace the nonlinear equilibrium path to the first critical point. The critical point can be a bifurcation or a limit point. But unlike the Riks/Wempner method, the Newton/Raphson method can not be used to pass through the limit point to trace post-buckling responses. The passing of a critical point is indicated by the appearance of a negative eigenvalue. "A nonlinear analysis" described in other chapters is based on the modified Riks/Wempner method.

2.2 Combined Analysis

A nonlinear analysis, which is based on the Newton/Raphson method, is applied to compute equilibrium points and combined with linear eigenvalue buckling predictions to obtain an estimate of the critical load. The method proceeds as follows (Holzer, Wu, and Tissaoui, 1991):

1. Apply a base load ${}^{b}p$ for a nonlinear analysis to obtain the corresponding tangent stiffness matrix ${}^{b}K$:

$$ {}^{b}p = p_D + {}^{b}\lambda p_L \tag{1} $$

If $p_D = 0$, Eq. (1) reduces to a single load condition.

2. A "small" live load increment is applied to obtain a reference load ${}^{r}p$ and a nonlinear analysis is performed to compute the corresponding tangent stiffness ${}^{r}K$. The change in the stiffness ΔK between the base load and the reference load is expressed as

$$\Delta K = {}^{r}K - {}^{b}K \tag{2}$$

3. By the linear buckling theory, the change in stiffness is proportional to the change in load. If

$$p = {}^{b}p + \Delta\lambda p_L \tag{3}$$

then

$$K = {}^{b}K + \Delta\lambda\Delta K \tag{4}$$

4. At the critical load, the stiffness matrix K is singular. This condition corresponds to the eigenvalue problem.

$$({}^{b}K + \Delta\lambda\Delta K)\Delta u = 0 \tag{5}$$

The solutions $\Delta\lambda$ and Δu are the eigenvalues and the eigenvectors. The eigenvectors provide buckling mode shapes for the structure. Let $\Delta\lambda_{cr}$ be the smallest eigenvalue, the predicted buckling load is expressed as

$$p_{cr} = {}^{b}p + \Delta\lambda_{cr}p_L \tag{6}$$

or by Eqs. (1) and (6) as

$$p_{cr} = p_D + {}^{b}\lambda_{cr}p_L \tag{7}$$

where

$${}^{b}\lambda_{cr} = {}^{b}\lambda + \Delta\lambda_{cr} \tag{8}$$

2.3 Comparison

The results of the combined analyses are presented as critical load prediction curves. This curve is determined by selecting increasing values for ${}^{b}\lambda$ and computing the corresponding eigenvalues $\Delta\lambda_{cr}$.

The relation between the two nonlinear analysis procedures is illustrated in Fig. 2.1. The critical point, $\lambda = {}^{b}\lambda = \lambda_{cr}$, on the 45° line, $\lambda = {}^{b}\lambda$, is computed by the nonlinear analysis. We can also reach this point by extending the critical load prediction curve to intersect the 45° line.

According to previous experience, the initial point, ${}^{b}\lambda = 0$, can occassionally provide a sufficiently accurate prediction. But one can not tell whether this value is conservative or unconservative (Cook, 1989; Chang, 1980). It depends on the formulation of the stiffness matrix and the program chosen by the user.

ABAQUS is capable of estimating elastic buckling by eigenvalue extraction. The estimation is especially useful for stiff structures whose structural responses are elastic up to the estimated buckling load values.

2.4 Nonlinear Analysis With ABAQUS

Several parameters contained in ABAQUS control the accuracy and the rate of convergence for the nonlinear analyses. They are discussed in this section.

When an eigenvalue buckling estimate is made, the program calls for the numerical differencing between base load and reference load represent the differential stiffness. The magnitude of load

increment must be small enough for the difference to be a close approximation to the derivative, but not so small as to cause round-off problems. ABAQUS recommends the load increment to be about 1% of the estimated lowest critical load. The analyses are performed smoothly in this study with a load increment equal to 1% of the design snow load.

Three parameters, the maximum load proportionality factor, the maximum displacement of a node for a degree of freedom, and the maximum number of increments, can be used in ABAQUS to terminate a Riks analysis. Since the cost of performing a Riks analysis is much higher than that of an eigenvalue buckling prediction, there is a necessity to control these factors in order to reduce the expenses of stability analysis.

Convergence criteria for nonlinear analysis are determined by specifying an initial time increment (or initial load increment) for a time period of 1.0, a maximun time increment, a minimun time increment, a force equilibrium tolerance (PTOL), and a moment tolerance (MTOL).

A value of 0.05 for the initial time increment is usually adopted in this study. The force tolerance is suggested to be about 0.1% to 1% of actual forces and the guideline for choosing the moment tolerance is to multiply PTOL by a typical element length (ABAQUS). A value of 1% of dead load at node 1 (apex) is selected for PTOL in the analyses of the B32 model. While a value of 0.5% of dead load at node 1 is selected for PTOL in the analyses of the B33 models.

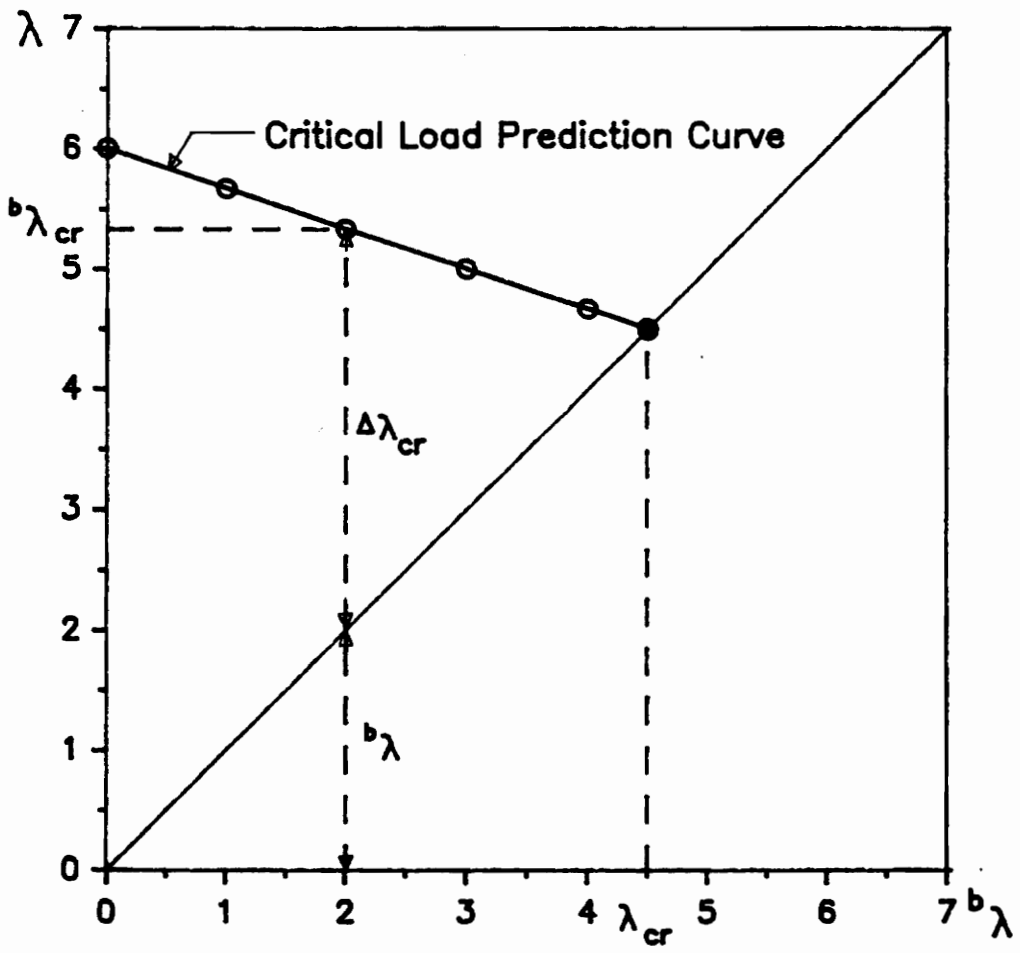

Figure 2.1. Buckling load prediction.

Chapter 3

MODEL AND LOAD

The Crafts Pavilion Triax dome built in Raleigh, N.C. was selected as the model applied in this study. It has a span of 1595 in., a rise of 212.345 in., a radius of curvature of 1600 in. The geometry of the dome is defined on a horizontal (pattern) plan. A network of equilateral triangles is projected onto the spherical surface of the dome by rays originating at the center of the sphere. Each equilateral triangle has a length of half the span divided by a triax number (Neal, 1973). The triax number is 3.4345 for the dome model.

Besides curved beams, the dome consists of a decking supported by curved purlins, and a steel tension ring. The dome is cyclically symmetric and composed of six identical sectors. The dimensions of the members are shown in Fig. 3.2(a).

A dome consists of hundreds of members; it is impractical to divide each member into many finite elements. Since each beam is divided into two finite elements, the proper selection of the elements is important. Selection of elements is discussed in Section 3.1. Material properties and boundary conditions are discussed in Section 3.2 and Section 3.3.

Several types of loads, especially wind load, must be defined before performing analyses. Presure coefficients on domes from ECCS (1987) and wind pressure formulas from ANSI A58.1-1982 are combined to compute wind pressure on the dome. They are presented in Section 3.4. The methods used in generating nodal forces are discussed in Section 3.6.

In order to study the effects of the joint stiffness and the bracing, a modeling method is developed and discussed in Section 3.5.

3.1 Selection of Elements

Two models are used in the analyses. In the first model, all joints are assumed to be rigid. The contribution of the decking is not considered. The second model is discribed in Section 3.5.

There are seven types of space beam elements available in ABAQUS. Among them, a 3-noded, curved, isoparametric beam element, B32, is well suited for modeling the structural characteristics of a space frame. Shear deformation can be significant in timber beams because the ratio of the longitudinal elastic modulus to the shear modulus is high.

The B32 beam element is based on Timoshenko's beam theory, it can take into account axial, biaxial bending, torsional, and shear deformations. It uses quadratic interpolation for discretization. The steel tension ring is modeled as straight truss elements to eliminate eccentric ring moments. This model of the dome is designated as the B32 model.

3.2 *Material Properties*

The glulam beams and purlins are classified as E-rated 56 southern pine (NDS, 1986). Their Young's modulus is taken as $E = 1{,}800{,}000$ psi. Since tabulated shear modulus for glulam beams is not available, the shear modulus $G = 160{,}000$ psi is obtained from torsion tests of small glulam samples (Davalos, 1989). The material is considered continuous, homogeneous and transversely isotropic.

ABAQUS requires the user to specify values for Young's modulus E and Poisson's ratio ν; the program computes the shear modulus from the equation

$$G = \frac{E}{2(1+\nu)}$$

and by

$$\nu = \frac{E}{2G} - 1$$

a value of 4.625 for Poisson's ratio is provided for ABAQUS.

The maximum parallel to grain stresses for longleaf pine obtained from the Wood Handbook (1987) are applied to check the maximum stresses acquired from nonlinear analyses of several models. These maximum stresses are the proportional limit for compression (5900 psi), the proportional limit for tension (8790 psi), the ultimate compressive stress (8470 psi), the ultimate tensile stress (14500 psi), and the ultimate shearing stress (1510 psi). A Young's modulus of 29,000,000 psi and a Poisson's ratio of 0.3 are provided for the steel tension ring.

3.3 Boundary Conditions

Boundary constraints must be applied to remove the dome's rigid body motion. A simple method, which had been used by Huang (1989), is adopted in the dome model. First, constraints in the Z-direction are applied to all nodes along the perimeter of the dome base to remove the rigid body motion in the vertical direction. Then, constraints in the X-direction are applied to two nodes, 38 and 50, at the intersections of the ordinate and the base ring. In addition, constraints in the Y-direction are applied to two nodes, 44 and 56, at the intersections of the abscissa and the base ring (Fig. 3.1). Thus, rigid body motion in both X and Y directions is removed and the rotation about Z axis is automatically eliminated.

3.4 Design Loads

Four types of loads and their combinations are included in the linear and nonlinear analyses. The design values of the dead load, live load, and snow load are presented in Sections 3.4.1 and 3.4.2. The design wind load for domes, which is not available from U.S. codes, is discussed in Section 3.4.3.

3.4.1 Dead Load

The dead load consists of the weight of structural members, such as the glulam beams and purlins, the steel connectors, the tongue-and-groove decking, insulation and roofing materials, and permanent electrical and mechanical fixtures. The dead load for the dome models is estimated as 2 psf

of beams and purlins, 5 psf of 2″ decking and 9 psf of steel connectors, roofing, and insulation materials, with a total weight of 16 psf (Davalos, 1989).

3.4.2 Live Load

The roof live load should be considered in the analyses of the dome. According to Timber Construction Manul (AITC, 1985), in no case should the design roof live load be less than the tabulated minimum live loads as specified by ANSI.

The live load for the dome is 20 psf computed from ANSI A58.1-1982, Section 4.10. It accounts for the weight imposed over the structure during construction, roofing and reroofing, and firemen with their equipment in the event of fire (Davalos, 1989). The snow load, which can be obtained from AITC manual, is of the same value as that of the live load.

3.4.3 Wind Load

Despite some deficiencies mentioned by Baker (1984), the ECCS pressure coefficients on domes are the best available and simple to apply. The ECCS specifies pressure coefficients at three points A,B,C along the midsection of the dome in the wind direction as shown in Fig. 3.3. The values between points A,B,C can be obtained by linear interpolation. The pressure along any section nomal to the wind is taken to be constant. The basic wind speed and equations for wind pressure calculations are obtained from ANSI. The wind pressure of the dome is computed as follows:

1. Use Fig. 3.3 from ECCS and linear interpolation to determine external pressure coefficients. Specifically, for

f/d = 212.3 / 1593 = 0.133

and

h/d = 180 / 1593 = 0.113

One obtains

C_p (at pt. A) = -0.25

C_p (at pt. B) = -0.48

C_p (at pt. C) = -0.11

2. The location of the dome is at Raleigh, N.C. Apply Fig. 1 in ANSI A58.1-1982, p.36, to obtain the basic wind speed V of 80 mph.

3. The dome is characterized by having exposure C (ANSI 6.5.3.1), category II (ANSI Table 1, p.24), and an importance factor I = 1.07 (ANSI Table 5, p.28).

4. For mean roof height = Z = (212.3/2 + 180)/12 = 23.85 ft. and exposure C, one obtains from ANSI Table 6, p.28:

K_z = 0.87 + 0.06(3.85/5) = 0.92

G_h = 1.29-0.02(3.85/5) = 1.28

where

K_z = velocity pressure exposure coefficient, and

G_h = gust response factor

5. Compute velocity pressure q_z by Eq. (3.1) (ANSI 6.5, Eq. (2), p.15):

$$q_z = 0.00256 K_z (IV)^2 \tag{3.1}$$

$$q_z = 0.00256(0.92)(1.07 \times 80)^2 = 17.26\, psf$$

6. By using the Table 9 in ANSI A58.1-1982, one obtains the internal pressure coefficient GC_i = 0.25.

7. Compute wind pressure on the dome by Eq. (3.2) (ANSI Table 4, p.27):

$$p = qG_hC_p - q_h(GC_i) \tag{3.2}$$

for $q = q_h = q_z$

$$p = q(G_hC_p - GC_i) \tag{3.3}$$

Apply Eq. (3.3):

at pt. A C_p = -0.25,

p = 17.26 (1.28(-0.25) - 0.25) = -9.84 psf

at pt. B C_p = -0.48

p = 17.26 (1.28(-0.48) - 0.25) = -14.92 psf

at pt. C C_p = -0.11

p = 17.26 (1.28(-0.11) - 0.25) = -6.75 psf

The wind pressures along the line connecting points A, B, and C can be obtained by linear interpolation (Fig. 3.4(a)). The negative pressure means that the dome is subjected to suction.

3.5 *Stability Study Modeling*

Investigating the effects of the joint stiffness and the bracing on the stability of the dome is the major purpose of this study. In order to vary joint stiffness, a connector element has to be added to both ends of each beam. The connector element has a length determined by the size of the cylindrical hubs which connects six elements at a node. The joint stiffness is modeled by specifying a percentage of the moments of inertia of the beam to the connector elements. A general beam section (ABAQUS) is used for the connector elements. It permits us to bypass the numerical integration across the section and allows us to input cross sectional properties directly. The ABAQUS input data for a 5x11 in. beam with 50% joint stiffness and units of in., lb are:

```
*BEAM GENERAL SECTION, SECTION = GENERAL, ELSET = EL1243
55.00, 0., 0., 227.2917, 0., 57.29167, 334.5833
0.689249, -0.585372, -0.426937
1800000.0, 160000.0, 0., 0.
*SECTION POINTS
-2.50, -5.50, 2.50, -5.50, -2.50, 5.50, 2.50, 5.50
```

The B33 beam element is adopted for both beams and connector elements in the second dome model. A program was written to compute the additional nodal coordinates (Appendix A). The B33 beams, which are based on the Bernoulli/Euler beam theory, neglect shear deformations and use cubic interpolation for discretization.

The function of a bracing is to simulate the contribution of the decking which provides lateral support to the beams. It is represented as a 2-node truss element.

The purlins transmit the loads from the decking and provide lateral support to the beams. They are modeled as a 2-noded truss element to simulate the actual beam-purlin joints. The dome model is designated as the B33 model (Fig. 3.5).

3.6 Load Generation

The load-carrying capacity of the decking is not taken into account. For the B32 model, each triangle consisting of three beams and a purlin is considered as a panel. Since the radius of curvature of the dome is relatively large, each panel can be treated as a flat triangle.

The uniformly distributed loads on the decking are transformed into distributed member loads by assigning load tributory areas to each panel (Fig. 3.2(b)). Then the distributed member loads are discretized into nodal forces by a finite element approach which is consistent with the formulation of the isobeam element.

For the B33 model, another procedure is applied. The nodal forces are generated by using shell elements (Fig. 3.4(b)), STRI3, which are formed by connecting three nodes with I-DEAS (SDRC, 1986; Broyles, 1990).

First, all nodes of the dome are fixed. Next, pressure in the opposite sense of the actual pressure is applied in a linear analysis to compute the reactions of all nodes. Finally, the reactions, which serve as nodal forces, are applied to the corresponding nodes.

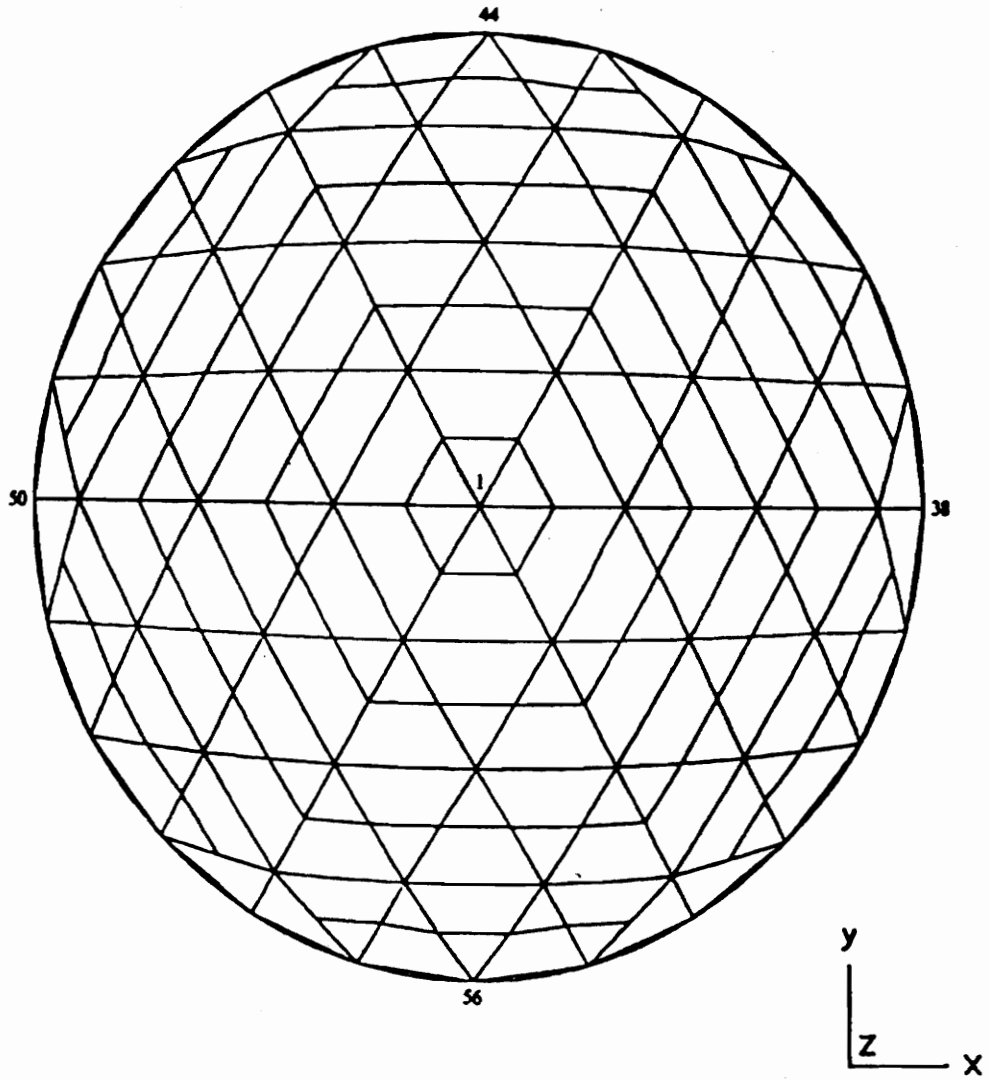

Figure 3.1. Triax dome model

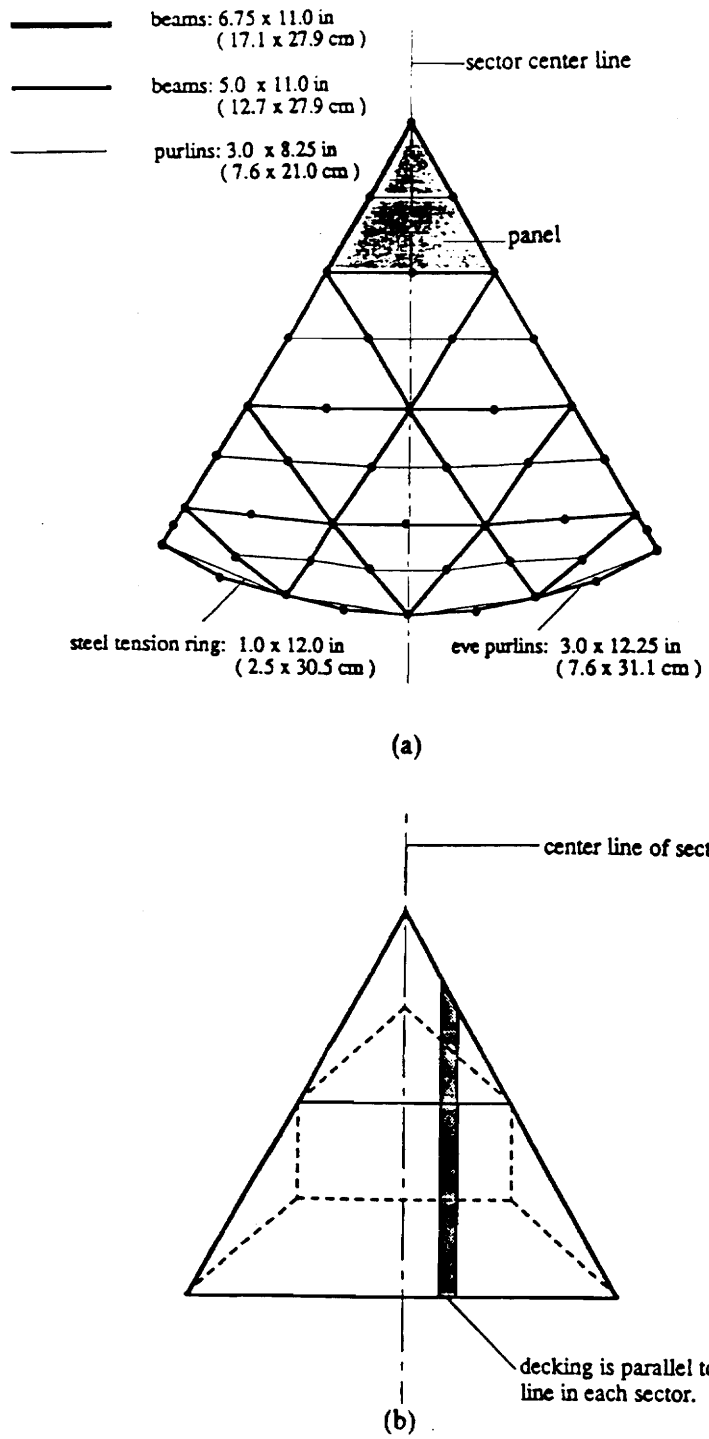

Figure 3.2. (a) Dimensions of the members of the dome model; (b) Tributory areas of one panel.

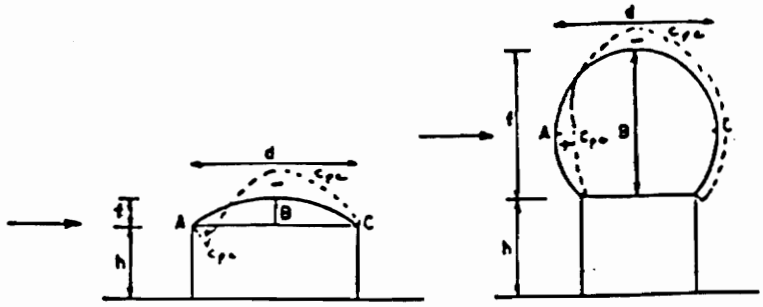

C_{pe} is constant along arcs of circles, intersections of the sphere and of planes perpendicular to the wind: it can be determined as a first approximation by linear interpolation between the values in A, B and C along the arcs of circles parallel to the wind.

In the same way, the values of C_{pe} in A if $0 < h/d < 1$ and in B or C is $0 < h/d < 0,5$ can be obtained by linear interpolation between the values read on the figure.

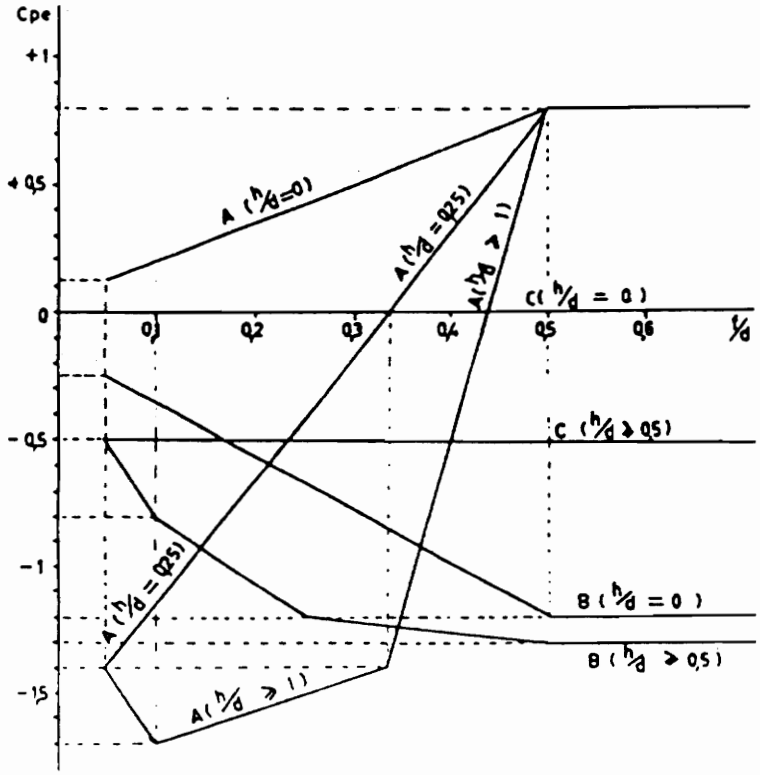

Figure 3.3. ECCS wind pressure coefficients for domes.

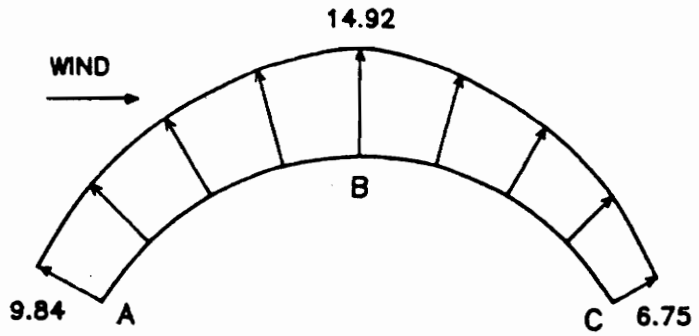

(a)

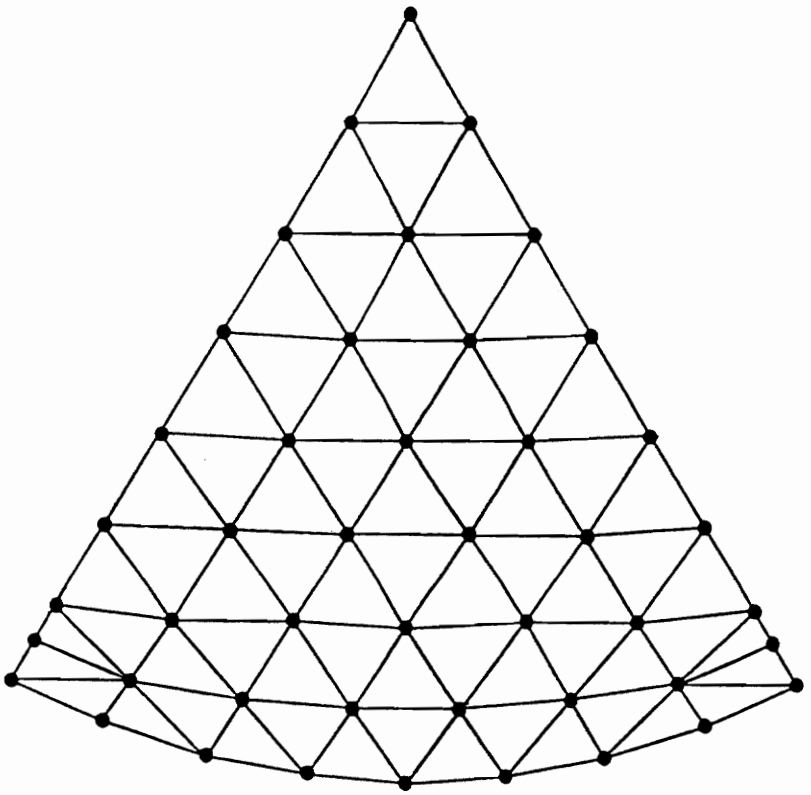

(b)

Figure 3.4. (a) Wind pressure distribution for the dome model; (b) Shell elements of one sector.

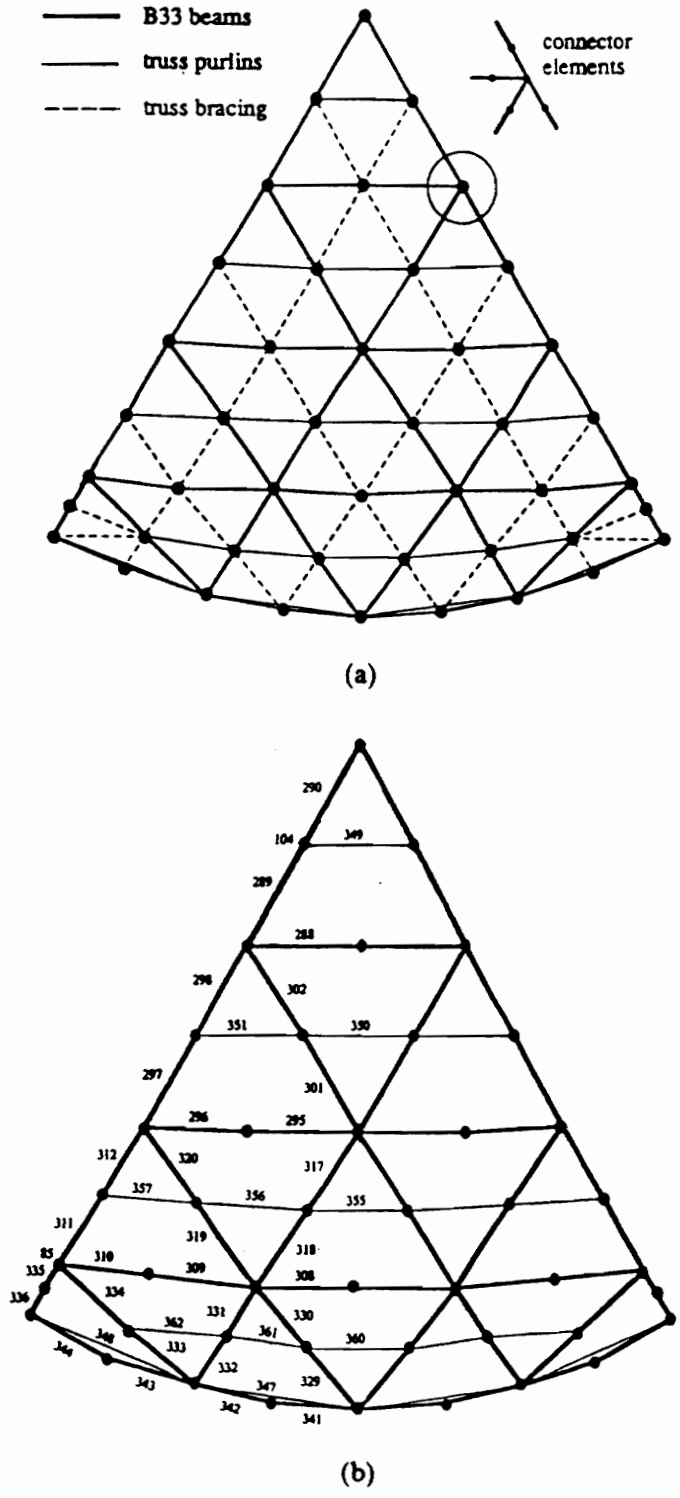

Figure 3.5. (a) One sector of the B33 model; (b) B33 elements of one sector for stress checking.

Chapter 4

ANALYSIS OF B32 MODEL

According to Timber Construction Manual (AITC, 1985), four load combinations must be included in the analyses. These load combinations are dead load and cyclically symmetric snow load over the entire dome, the inner half and the outer half of the dome as well as dead load and snow load over half of the dome.

Since the critical load condition in the linear range is uniform snow load over the entire dome (Huang, 1989), two load cases of inner and outer snow loads are omitted in the linear analyses. But nonlinear analyses for four load combinations are performed. The effects of load duration on the material properties are not considered in this study. The design dead load is 16 psf and the design snow load is 20 psf. A detailed discription of this model is presented in Sections 3.1, 3.2, and 3.3.

4.1 Linear Analysis

For the load condition of dead load and uniform snow load, the maximum compressive stress of the beams is 1505 psi at element 189, node 32, and the maximum tensile stress of the beams is 1170 psi at element 254, node 188. The vertical displacement at apex (node 1) is 1.58 in.

For the load condition of dead load and snow load over the lower half dome, the maximum compressive stress of the beams is 1552 psi at element 218, node 170, and the maximum tensile stress of the beams is 1242 psi at element 245, node 28.

All these maximum stresses are below the proportional limit and smaller than the allowable stresses which are 2400 psi for compressive stress and 1550 psi for tensile stress (Huang, 1989). The nodes and elements mentioned above are shown in Fig. 4.1(a).

4.2 Nonlinear Analysis

A nonlinear analysis and a combined analysis are carried out for each load combination. The results of nonlinear (Riks) analyses provide us the information where a critical point had been passed. For the load combination of dead load and uniform snow load, the critical load parameter λ_{cr} is between 3.69 and 3.87. For the load combination of dead load and inner snow load, λ_{cr} is between 4.01 and 4.19. For the load combination of dead load and outer snow load, λ_{cr} is between 5.14 and 5.22. For the load combination of dead load and half snow load, λ_{cr} is between 5.87 and 5.90.

The critical load parameters obtained by using critical load prediction curves should be in accordance with the results of Riks analyses. An example of the computation of the buckling load pre-

diction for the load condition of uniform snow load is presented in Table 4.1(a). The critical load prediction curves for the load conditions of uniform snow load, inner snow load, outer snow load, and half snow load are shown in Fig. 4.2 and Fig. 4.3.

4.3 Maximum Stress

A method to seperate the maximum stress into the axial and biaxial bending components is applied extensively in this study. This method was first introduced by Holzer and Huang (1989). It is presented briefly in this section.

Consider a cross section of an element subjected to an axial force and biaxial bending moments as shown in Fig. 4.1(b). The points 1, 2, 3 and 4 are at the four corners of the cross section. They correspond to the section points 1, 5, 21 and 25 in ABAQUS.

The axial stresses with a value A are developed at four points when an axial force is applied. The bending stresses with a value B_1 at points 3 and 4, and a value $-B_1$ at points 1 and 2 are developed if a moment is applied about the local 1 axis of the element. The bending stresses with a value B_2 at points 1 and 3, and a value $-B_2$ at points 2 and 4 are developed if a moment is applied about the local 2 axis of the element.

Let the resultant stresses at the four corners be S1, S2, S3, and S4. We can compute A, B1, and B2 by the following three equations.

$$A = \frac{1}{4}(S1 + S2 + S3 + S4) \tag{4.1}$$

$$B1 = \frac{1}{4}(-S1 - S2 + S3 + S4) \tag{4.2}$$

$$B2 = \frac{1}{4}(S1 - S2 + S3 - S4) \tag{4.3}$$

4.4 Discussion

In addition to buckling pressures, buckling modes and material behavior are also our major concerns. The results from critical load prediction curves are in good agreement with the results of nonlinear(Riks) analyses. However, of particular interests are the buckling modes of uniform snow over the entire dome and over half the dome. The equilibrium paths of node 138 for uniform snow over the entire dome are shown in Fig. 4.4(a). And the equilibrium paths of node 454 for snow over half the dome are shown in Fig. 4.4(b).

These figures indicate that at the predicted buckling load, the fundamental equilibrium path is intersected by a secondary path. This means for the two load cases, buckling loads are at the bifurcation points and the dome model fails by lateral buckling of the beams.

This form of twist buckling is further proved by checking the maximum stresses (Table 4.1(b)) and plotting the buckling modes (Fig. 4.5) for the uniform snow over the complete dome and over half the dome.

For snow over the complete dome, the bending stress B2 is larger than the bending stress B1. For snow over half the dome, which failed by local stress concentration, the lateral bending stress is twenty times as large as the primary bending stress. The maximum stresses for snow over the complete dome remain in the elastic range. On the contrary, the stresses in some elements due to snow over half the dome exceed the ultimate compressive and tensile stresses. Consequently, elastic instability does not dominate the critical state for snow over half the dome.

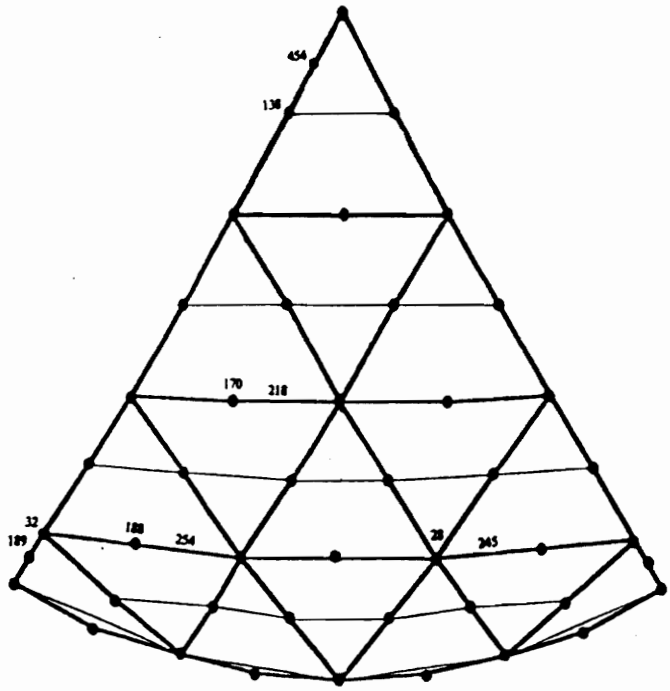

(a)

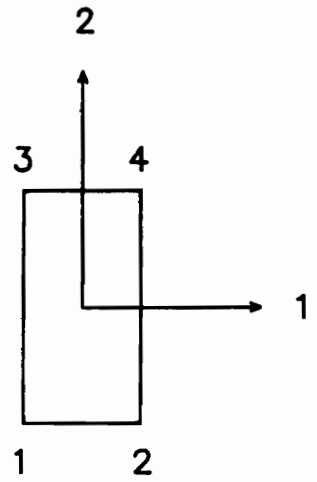

(b)

Figure 4.1. (a) B32 elements of one sector for stress checking; (b) Element cross section for stress checking.

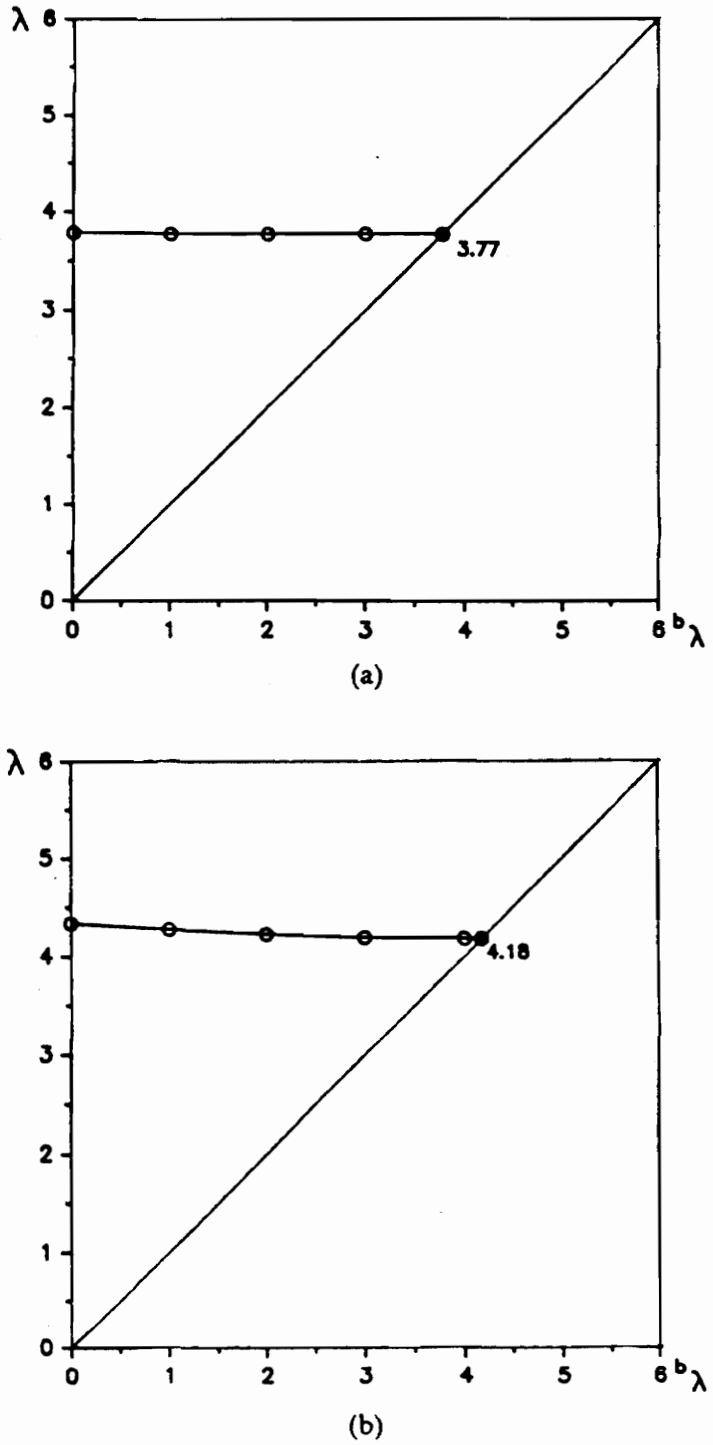

Figure 4.2. Critical load prediction curves for (a) snow over the entire dome and (b) snow over inner half of the dome.

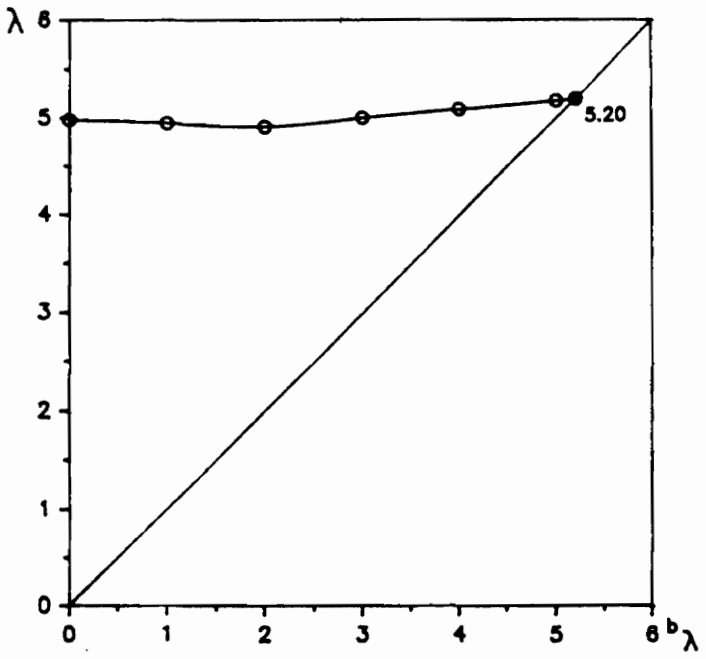

(a)

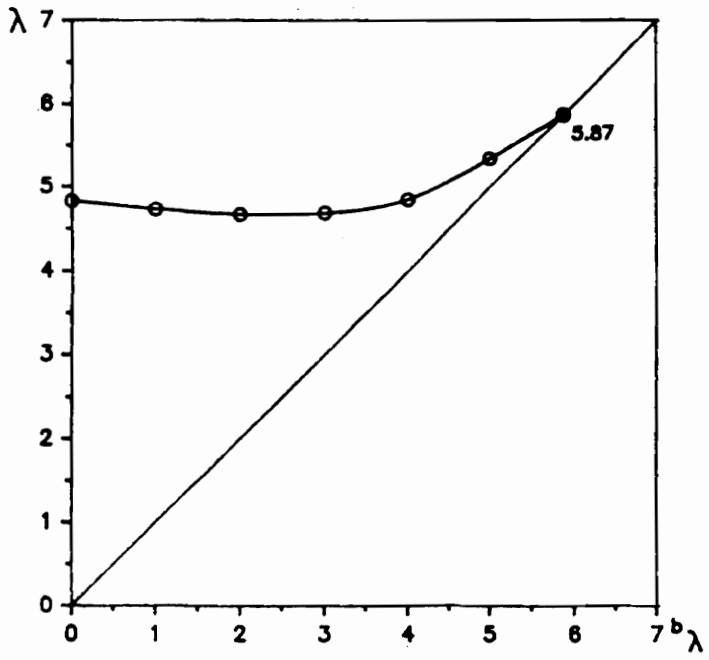

(b)

Figure 4.3. Critical load prediction curves for (a) snow over outer half of the dome and (b) snow over half the dome.

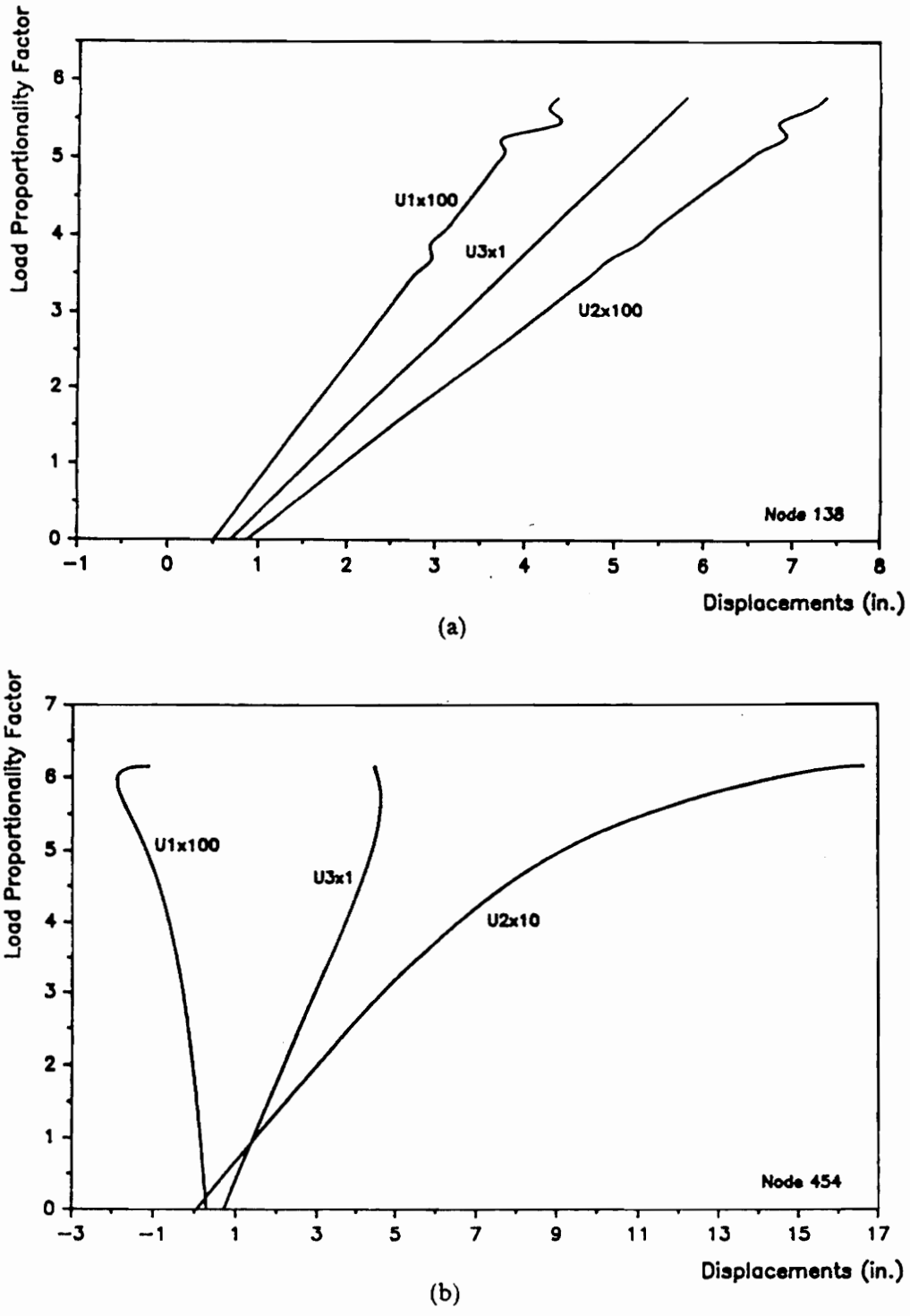

Figure 4.4. Equilibrium paths for (a) snow over the entire dome and (b) snow over half the dome

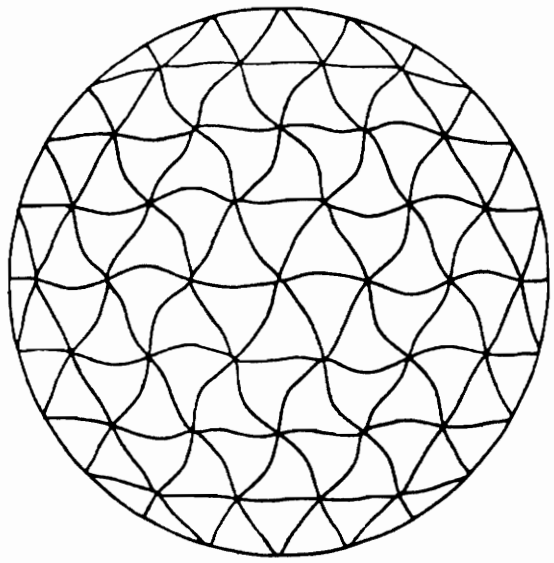

(a)

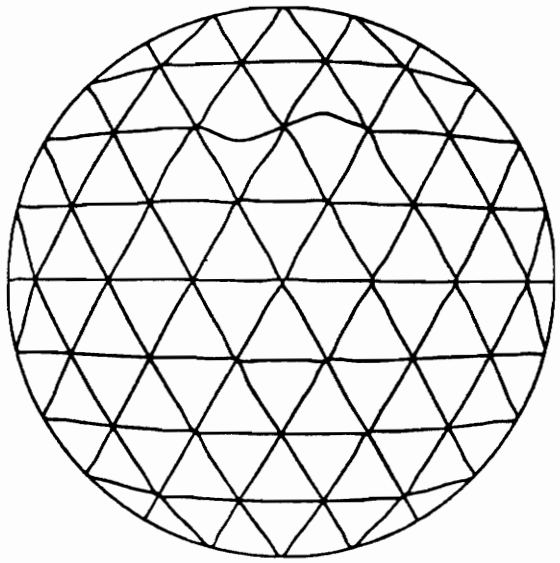

(b)

Figure 4.5. Buckling modes for (a) snow over the entire dome and (b) snow over half the dome.

Table 4.1(a) Buckling Load Prediction for Uniform Snow Load (unit:psf)

No.	${}^b\lambda$	β	P_l	C_{cr}	$\Delta\lambda_{cr}$	${}^b\lambda_{cr}$	P_{cr}
1	0.0	0.01	16	378.92	3.789	3.799	91.78
2	1.0	0.01	36	277.82	2.778	3.778	91.56
3	2.0	0.01	56	177.25	1.773	3.773	91.46
4	3.0	0.01	76	77.185	0.772	3.772	91.44

Note: $p_l = p_D + {}^b\lambda p_L$

$p = p_l + Cp_j$

$p_j = \beta p_L$

$p_{cr} = p_D + {}^b\lambda_{cr} p_L$

$\Delta\lambda_{cr} = \beta C_{cr}$

${}^b\lambda_{cr} = {}^b\lambda + \Delta\lambda_{cr}$

p_D = 16 psf and p_L = 20 psf.

C_{cr} is the smallest eigenvalue.

Table 4.1(b) Maximum stresses just before buckling for B32 models (unit:psi)

Model	Max. Compression of Beams	Max. Tension of Beams	Max. Compression of Purlins	Max. Tension of Purlins	Max. Tension of Steel Bars
Snow Over the Entire Dome	A = -765.6 -4248. B1= 1396.6 B2=-2085.9	A = -392.5 2989. B1=-1564.6 B2= 1816.9	-3807.	3054.	29289.
Snow Over Half of Dome	A =-2174.5 -21003. B1= -897.0 B2=17941.5	A =-2174.5 16664. B1= -897.0 B2=17941.5	-10179.	8369.	38924.

Chapter 5

EVALUATION OF B33 MODEL

Before studying the effects of the joint stiffness and the bracing, the new B33 model must be checked against the B32 model. We are not certain if the analyses of the B33 model, which neglects shear deformation, can provide satisfactory results. And we don't know how well the model can converge when the connector elements, whose length is only 2% of the beam span, are added to the beams.

Three linear analyses for three B33 models are performed first for the load combination of dead load and uniform snow load.

5.1 Linear Analysis

The first model is a rigid space frame obtained by deleting the mid node of the B32 beam element. The second model is generated by adding connector elements, which have 100% joint stiffness, to

all beams of the first model. The third model is similar to the second model except the purlins consist of truss elements. Comparison between B32 and B33 models begins with the first B33 model.

There are two sets of nodal forces for the first model. The first set of nodal forces was generated by imposing snow load over the spherical surface of the dome. This procedure was used in generating nodal forces for the B32 model. The second set of nodal forces was generated by imposing snow load over the horizontal projection of the dome.

The total load of the first set is 3.83% larger than that of the second set. The second nodal force set is also applied to the second and the third B33 models.

Stress comparison for the corresponding elements between the B32 model and the B33 model 1 did not provide us significant information on the similarity of the two models. And comparison of the reactions between the two models did not demonstrate distinct differences between them.

For the nodal force set 1, Considering each panel as a flat triangle results in a total reacion 1.35% less than the actual loads. I-DEAS provides us better results with a total reaction 0.35% less than the actual loads for the same nodal force set.

For the first set of nodal forces, the comparison of nodal deflections in the vertical direction indicated that the B33 model 1 has a deflection 1.0% on an average less than that of the B32 model. For the second set of nodal forces, the comparison of nodal deflections in the vertical direction indicated that the B33 model 1 has a deflection 3.8% on an average less than that of the B32 model.

A simple comparison of the vertical deflections at the apex (node 1) yields 1.58 in. for the B32 model, 1.50 in. for the B33 model 1 with nodal force set 1, 1.50 in. for the B33 model 1 with nodal force set 2, 1.50 in. for the B33 model 2, and 1.51 in. for the B33 model 3. Although adding connector elements to the beams tends to soften the dome model, but it's effect is less than that of re-

placing B32 beams with B33 beams. We come to the conclusion that it is feasible to replace the B32 beam element by the B33 beam element in the dome models.

The B33 model 2 modeled the purlin as a beam and the B33 model 3 modeled the purlin as a truss element. However, similarities exist between them. They both have the same maximum stresses for the beams and steel tension rings.

A detailed stress comparison between corresponding elements for the three B33 models has been made. The result is presented in Appendix B.

In ABAQUS, the program will compute the cross sectional properties automatically by integration if a beam SECTION = RECT is specified. However, the general beam section is essential for the modeling of joint stiffness. The user must provide cross sectional properties. A linear analysis with beam SECTION = RECT has been performed for the B33 model 2. The results are identical to that with beam SECTION = GENERAL for the same model.

5.2 Nonlinear Analysis

The results of nonlinear analyses provide us a positive assessment for the B33 model.

For the B32 model, the critical load parameter is 3.77. For the second B33 model, the nonlinear (Riks) analysis indicates that the critical load parameter is between 3.70 and 3.88. With the aid of the combined analysis, the critical load parameter is predicted to have a value of 3.78. Compared with the B32 model, the B33 model is accurate enough.

The nonlinear analyses performed for the B33 model 3 resulted in a critical load parameter of 3.30. A comparison between the second and the third B33 models indicates that the rotational stiffness

of the purlin reduces the lateral twist of the beam and increases the buckling pressure. The effect of the stiffness in the beam-purlin joint on the stability of the dome is significant; however the actural beam-purlin joint is pinned.

5.3 Wind Load Effect

Load combinations of dead load, wind load and snow load must be considered in the analyses of glulam domes as required by AITC (1985). In this section, two load combinations of dead load and wind load, and dead load, wind load, and snow load over half the dome are applied. The design wind pressures are shown in Fig. 3.3(a). The reactions in the directions of X, Y, and Z, which are generated by applying shell elements, have been applied to all nodes for analyses.

The results of linear analysis for the load combination of dead load and wind load showed that this load condition will not control the dome design. The vertical component of the sum of dead load and wind load is downward and smaller than the dead load. Considering the snow load over the entire dome, the effect of the sum of dead load, wind load, and snow load over the entire dome is smaller than that of dead load and snow load over the entire dome.

The results of linear analysis for the load combination of dead load, wind load, and half snow load have the same result. The effect of the sum of dead load, wind load, and half snow load is less than that of dead load and half snow load. Although the maximum tensile stress occurs at the unloaded half of the dome, it is not large enough to control the design of the dome.

The same conclusions should be applicable to the load conditions of inner snow load and outer snow load. The maximum stresses in beams, purlins and steel tension bars for four models with various load combinations are shown in Table 5.1.

A nonlinear analysis for the B33 model 1 with load combination of dead load, wind load, and half snow load has been carried out. The nonlinear analysis for this load condition terminated at a load proportionality factor of 6.45 without the appearance of a negative eigenvalue. This means that the value of the critical load parameter for this load condition is larger than that of the four load conditions in the B32 model.

According to the discussions mentioned above, we can reach a conclusion that wind load is not an important factor in the design of the dome if the calculation of wind pressure is correct.

Table 5.1 Maximum stresses of linear analyses (unit: psi)

Model	Load Condition	Max. Compression of Beams	Max. Tension of Beams	Max. Compression of Purlins	Max. Tension of Purlins	Max. Tension of Steel Bars
B32 Model	Dead Load + Unif. Snow Load*	-1505.0	1170.0	-1354.0	1271.0	11379.
B33 Model 1	Dead Load + Unif. Snow Load*	-1559.0	992.1	-635.8	878.9	11367.
B33 Model 1	Dead Load + Unif. Snow Load**	-1494.0	970.0	-613.7	850.0	11026.
B33 Model 2	Dead Load + Unif. Snow Load**	-1534.0	1232.0	-381.3	349.8	11045.
B33 Model 3	Dead Load + Unif. Snow Load**	-1535.0	1229.0	-322.9	63.0	11045.
B32 Model	Dead Load + Half Snow Load*	-1552.0	1242.0	-1530.0	1291.0	10392.
B33 Model 2	Dead Load + Half Snow Load**	-1623.0	1159.0	-668.3	422.7	10086.
B33 Model 3	Dead Load + Half Snow Load**	-1639.0	1159.0	-242.6	56.9	10085.
B33 Model 1	Dead Load + Wind Load	-489.0	447.7	-133.1	181.0	1857.0
B33 Model 1	Dead Load + Wind Load + Half Snow Load**	-1266.0	1105.0	-603.8	661.0	6882.0

Note: * Snow load on spherical surface of the dome.
** Snow load on horizontal projection of the dome.

Chapter 6

STABILITY INVESTIGATION

The third B33 model discribed in chapter 5 forms the basis for the modeling of the joint stiffness and the bracing. Purlins are modeled by truss elements. The joints are modeled by specifying a percentage of the moments of inertia I_{11}, I_{22}, and J of the beams for the connector elements while keeping the cross sectional area A unchanged. A bracing of truss elements is introduced to study the effect of the decking.

Linear, nonlinear, and combined analyses with two load conditions of uniform snow load and half snow load are performed for the models.

First, the dome is analyzed by modifying the moments of inertia of the connector elements to study the effect of the joint stiffness. Second, the dome is analyzed by changing the area of the bracing to simulate the contribution of the decking. Finally, the dome with fixed bracing area is analyzed by changing the joint stiffness to study the combined effect provided by the joints and the decking.

6.1 Models Without Bracing

Linear analyses are performed first to study the effect of flexible joints. For the load condition of snow load over the entire dome, joint stiffnesses of 100%, 75%, 50%, 25%, 7%, and 1% are assigned to the connector elements. The results are shown in Table 6.1(a).

For the load condition of snow over half of the dome, joint stiffnesses of 100% and 25% are assigned to the connector elements. The results are shown in Table 6.1(b).

Changing joint stiffness of the beam did not have much influence on the maximum design stresses of the dome. Compared with the maximum stresses of the model with rigid joints, the stress differences are within 10% for any model whose joint stiffness is reduced up to 75%.

Then an incremental iterative nonlinear analysis and a combined nonlinear/linear eigenvalue analysis are applied for the models with flexible joints.

For the load condition of uniform snow load, connector elements with joint stiffnesses of 100%, 75%, 50%, 25%, 7%, and 1% of the moments of inertia of the beams are modeled. The results are shown in Fig. 6.1 and Table 6.2(a).

For the load condition of half snow load, connector elements with joint stiffnesses of 100%, 50%, and 25% of the moments of inertia of the beams are modeled. The results are shown in Fig. 6.2 and Table 6.2(b).

Since the value of the critical load parameter for the load condition of uniform snow load determines the stability of the B32 model, a curve of critical load parameter vs. joint stiffness was plotted for this load condition (Fig. 6.6(a)). This curve can be used to predict the buckling load of the dome with flexible joints if the contribution of the decking is neglected.

After checking the critical load parameters for the models with 100%, 50%, and 25% joint stiffnesses, we found the ratios of λ_{cr} for flexible joints over λ_{cr} of rigid joints are 0.93 for 50% joint stiffness and 0.83 for 25% joint stiffness for the load conditions of uniform snow load and half snow load.

It appears that the joint stiffness has the same effect for both load conditions. And the load-carrying mechanism of the dome is not sensitive to uniform variations in the joint stiffness.

The maximum stresses of the models with 100%, 50%, and 25% joint stiffnesses were checked for two load cases. The results are shown in Table 6.3(a) and Table 6.3(b).

Since the lateral bending stress B2 is larger than the primary bending stress B1 for the two load conditions, the failure of the dome can be due to the lateral buckling of the beams. It is further demonstrated by checking the buckling modes (Fig. 6.3 and Fig. 6.4) and equilibrium paths (Fig. 6.5(a)) for some models. In order to have clear drawings, purlins are omitted in the buckling modes.

The buckling mode for the uniform snow load is bifurcation. The critical point for snow over half the dome is a limit point. The maximum compressive and tensile stresses for the uniform snow load is still below the proportional limit.

But for the load condition of snow over half the dome, the maximum compressive stresses are twice as large as the ultimate compressive stress and the maximum tensile stresses are between the proportional limit and the ultimate tensile stress. Elastic instability does not determine the critical state for this load condition.

6.2 *Models With Bracing*

Only two linear analyses with 100% and 25% joint stiffnesses are performed for each load condition. The results are shown in Table 6.1(a) and Table 6.1(b). Compared with the maximum stresses of the models without bracing, the maximum stresses of the models with bracing are lower. The maximum stresses of the models without bracing increase as the joint stiffness is decreased. But the effect of the bracing tends to reduce the maximum compressive stress for both load conditions when the joint stiffness is reduced.

Nonlinear analyses begin with the load condition of uniform snow load for a model with rigid joints and bracings. By changing the cross sectional area A of the bracing, a set of critical load parameters was generated. And a curve of critical load parameter, λ_{cr}, vs. bracing area, A, is shown in Fig. 6.6(b). Only a small A of 0.008 $in.^2$ is required to obtain the same value of critical load parameter as the B32 model has.

Two values of 0.1 $in.^2$ and 0.45 $in.^2$ for A are chosen for the load condition of snow over the entire dome. A value of 0.3 $in.^2$ for A is selected for the load condition of snow over half the dome.

With A equal to 0.1 $in.^2$ and 0.3 $in.^2$, two nonlinear procedures are applied for three models with 100%, 50%, and 25% joint stiffnesses. With A equal to 0.45 $in.^2$, a nonlinear analysis and a combined analysis for a model with rigid joints are perfomed.

Results presented include critical load prediction curves (Fig. 6.7, and Fig. 6.8) and tables (Table 6.2(a) and Table 6.2(b)), buckling modes (Fig. 6.9, Fig. 6.10 and Fig. 6.11), maximum stresses (Table 6.3(a) and Table 6.3(b)) and equilibrium paths (Fig. 6.12).

6.3 Discussion

In addition to buckling pressure and buckling mode, effects of the joint stiffness and the bracing on the response of the dome and material behavior are our major concerns. Two load conditions of snow over the entire dome and snow over half the dome are considered.

6.3.1 Uniform Snow Load

Table 6.3(a) indicates that the contribution of the bracing to the stability of the dome is more significant than that of the joint stiffness. For the case of A equal to zero, the critical load parameter is decreased by 17%, as the joint stiffness is reduced to 25%. By comparison, the critical load parameter is decreased by only 2.4% for a A equal to 0.1 $in.^2$ with the same reduction of joint stiffness. The bracing strengthens the global action of the dome and the premature twist buckling is suppressed.

This observation is supported by checking the maximum stresses of the dome just before buckling (Table 6.3(a)). The maximum compressive and tensile stresses remain nearly constant with changes in the joint stiffness. The maximum compressive stress has increased by about 150% and the maximum tensile stress has increased by about 50% compared with that of the models without bracing.

The maximum compressive stress exceeds the ultimate compressive stress by 15%, while the maximum tensile stress is still within the elastic range. The assumption of elastic instability must be revised.

After checking the equilibrium paths (Fig. 6.12(a)) of the three models with A equal to 0.1 $in.^2$, the buckling load of the dome is at the bifurcation point. However, it is close to the limit point.

The buckling modes (Fig. 6.9) indicate that the dome fails in the form of twist buckling of the beams. But for a model with a bracing area equal to 0.45 $in.^2$, the buckling mode (Fig. 6.10) shows that the lateral twisting of the beams has almost vanished and is replaced by vertical bending of the entire dome.

The maximum compressive stress is increased by 17% and the maximum tensile stress is reduced by 7% to reflect the increase in the area of the bracing. The equilibrium paths (Fig. 6.12(b)) indicate that the curve of each degree of freedom passes through the limit point.

6.3.2 Half Snow Load

The Table 6.2(b) demonstrates that the effect of the bracing is less dramatic for snow over half the dome than for snow over the entire dome. Compared to a decrease of 2.4% for the uniform snow load, the value of the critical load parameter is decreased by 7.5% for the half snow load as the joint stiffness is reduced to 25%. For the half snow load, the value of the critical load parameter is more sensitive to the variations in the joint stiffness than for the uniform snow load. The introduction of the bracing increases the maximum compressive stress by 5%, and reduces the maximum tensile stress by 35% for the model with rigid joints. In addition, a 12% increase of the maximum compressive stress and a 25% decrease of the maximum tensile stress are provided for the model with 25% joint stiffness (Table 6.3(b)). In contrast to the uniform snow load, the maximum compressive stresses show a little increase for the half snow load as the joint stiffness is reduced. It appears that the twist buckling of the beams is not a dominant factor for the stability of the dome with half snow load.

Examining Table 6.3(b), we observe that the maximum compressive and tensile stresses occurred at the same element. And the difference between maximum bending stress B1 and maximum bending stress B2 for the half snow load is about 11,000 psi, which is twice as high as that for the uniform snow load. Bending is a more significant component of the load-carrying mechanism for snow over half the dome.

The critical load parameter is at the limit point (Fig. 6.5(b)) provided by a Riks analysis. The buckling modes (Fig.6.11) indicate that the dome has failed by local stress concentration in the form of bending about the local 1 axis of some beams. Thus, the bracing can not overcome the nonuniform response introduced by the load over half the dome.

The maximum compressive stress exceeds the ultimate compressive stress by 110% and the maximum tensile stress lies between the proportional limit and the ultimate tensile stress. Thus, material properties beyond the proportional limit must be incorporated in the analyses.

The maximum stresses just before buckling of the bracings are also checked. For the load condition of half snow load, the maximum compressive stress is 26016 psi and the maximum tensile stress is 16831 psi for the model with a bracing area equal to $0.3in.^2$ and with rigid joints. For the load condition of uniform snow load, the maximum compressive stress is 27931 psi and the maximum tensile stress is 4546 psi for the model with a bracing area equal to $0.45in.^2$ and with rigid joints. At such high compressive stress, the bracings have already buckled. It is possible that the bracings share the pressure with beams. The modeling technique used to simulate the contribution of the decking has to be improved.

For the models without bracing, the value of the critical load parameter for the load condition of uniform snow load determines the stability of the dome. But the value of the critical load parameter for the load condition of half snow load decides the stability of the dome when the contribution of the decking is considered.

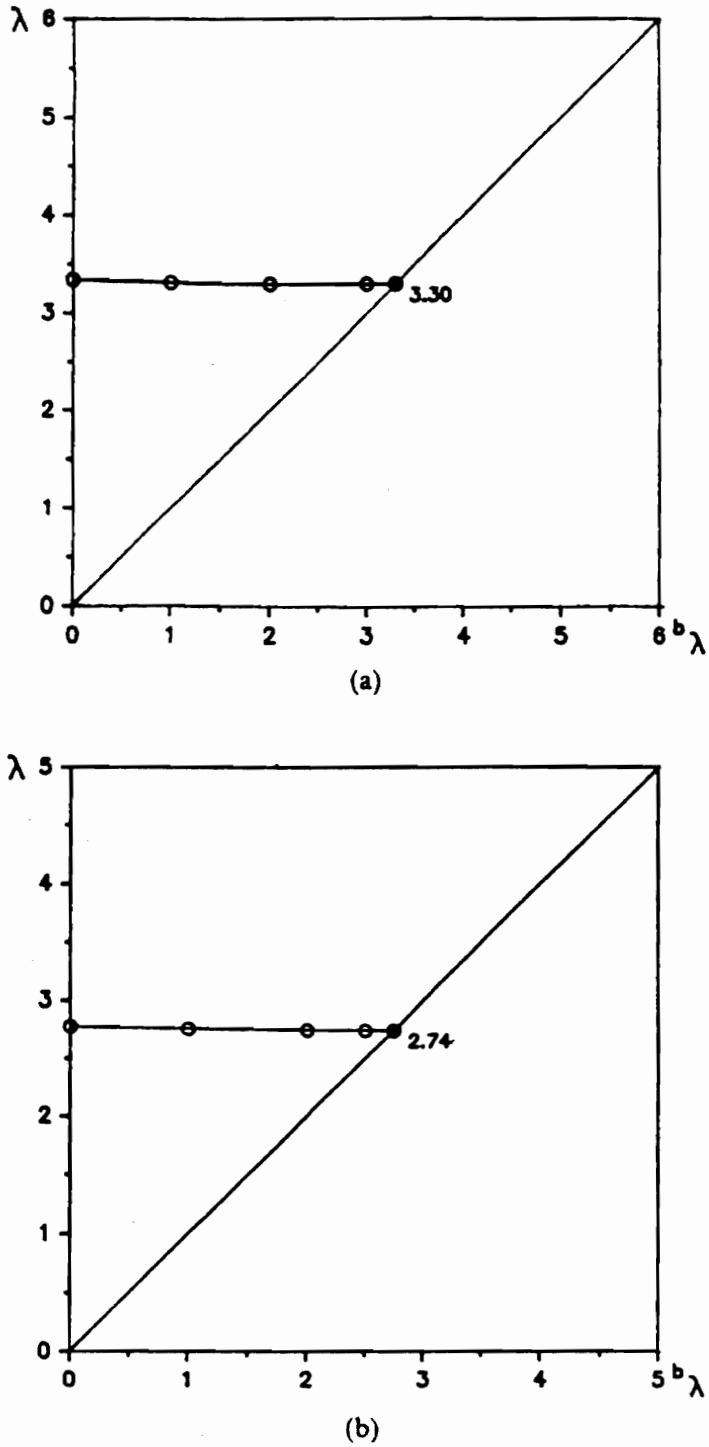

Figure 6.1. Critical load prediction curves for models without bracing and with (a)100%; (b)25% joint stiffnesses for uniform snow load.

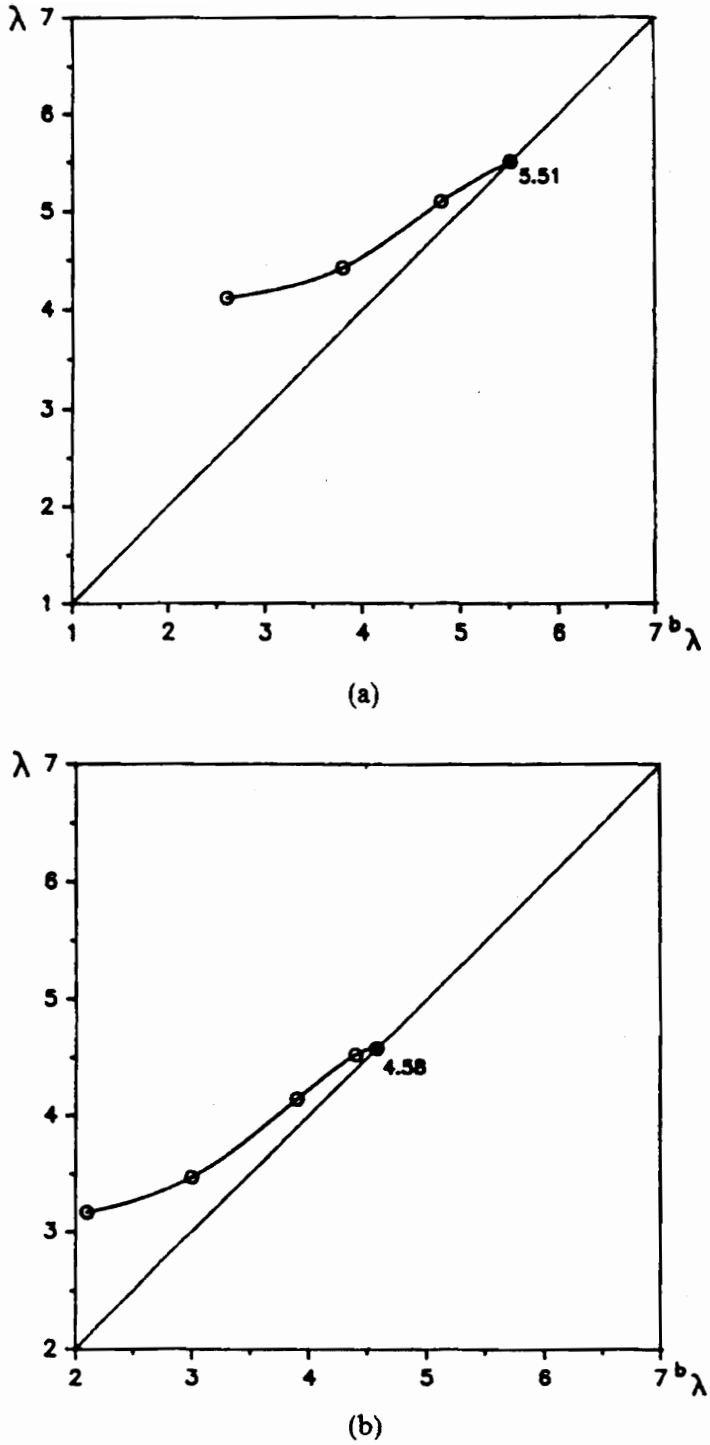

Figure 6.2. Critical load prediction curves for models without bracing and with (a)100%; (b)25% joint stiffnesses for half snow load.

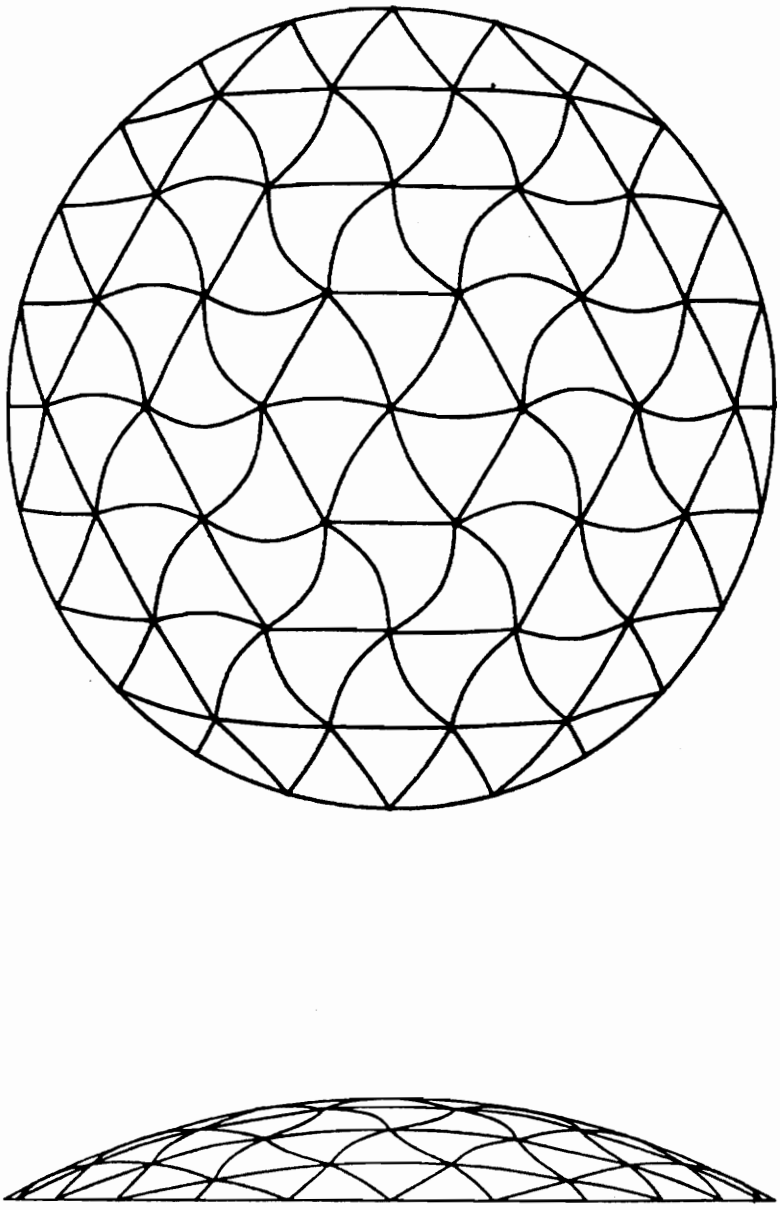

Figure 6.3. Buckling mode of the models with 100% and 25% joint stiffnesses for snow over the entire dome.

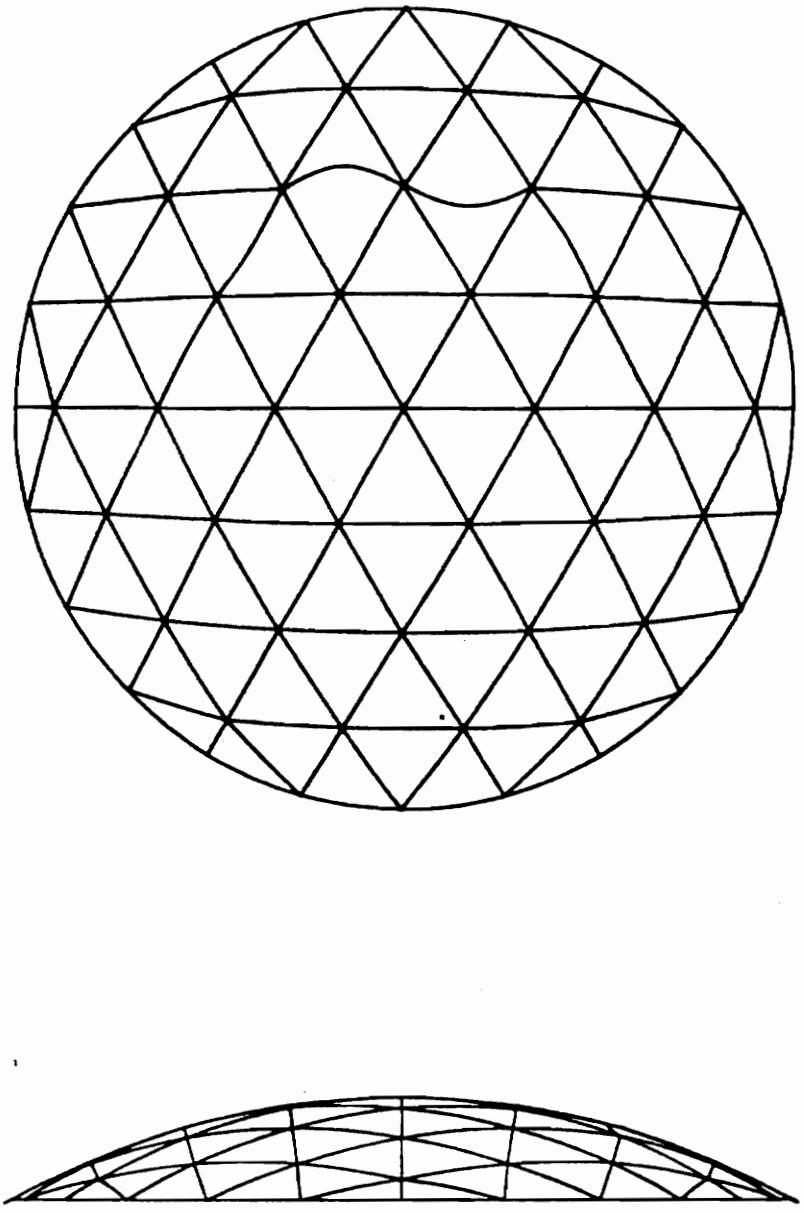

Figure 6.4. Buckling mode of the models with 100% and 25% joint stiffnesses for snow over half the dome.

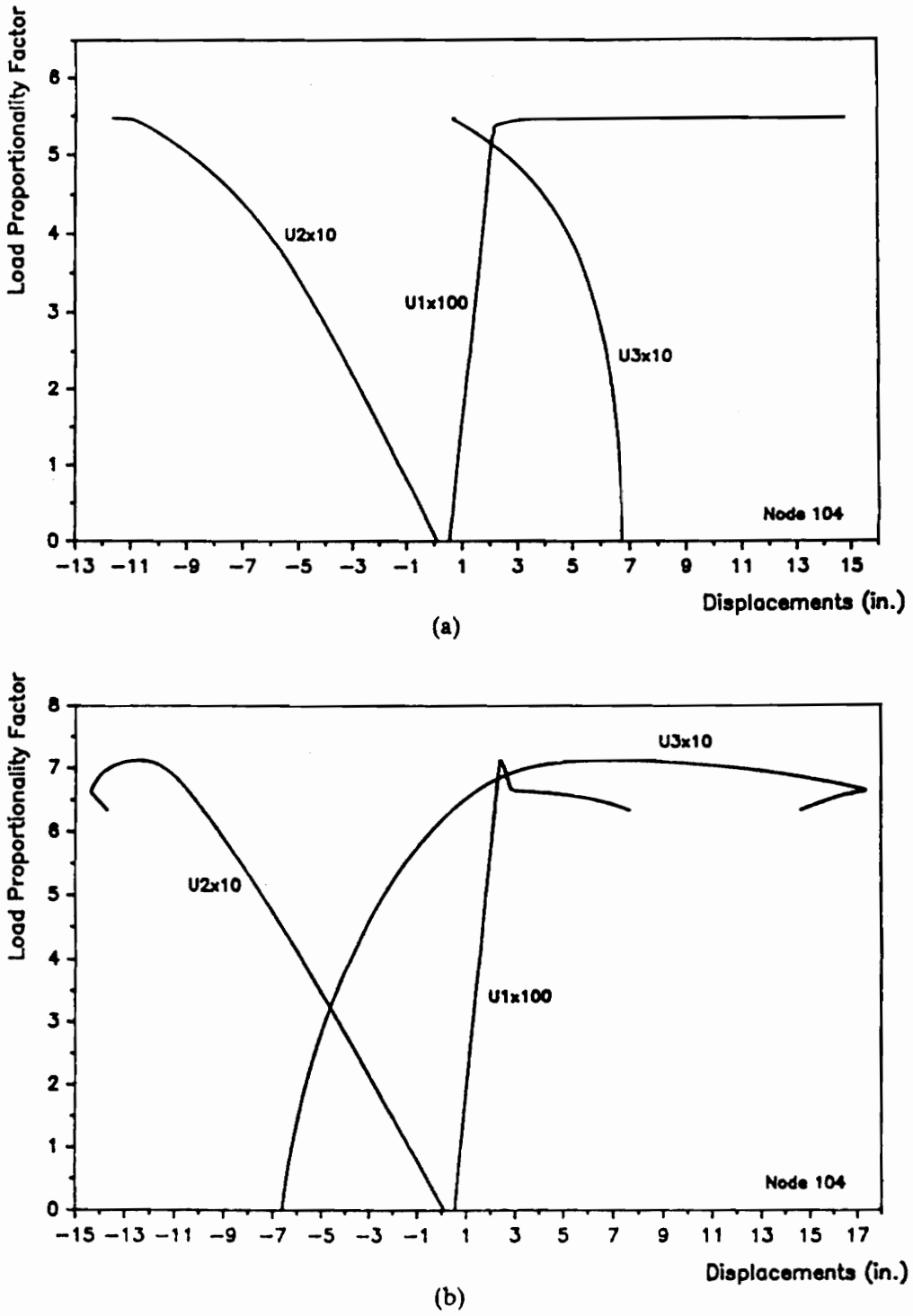

Figure 6.5. Equilibrium paths of the models with (a)rigid joints without bracing;(b)25% joint stiffness with bracing for half snow load.

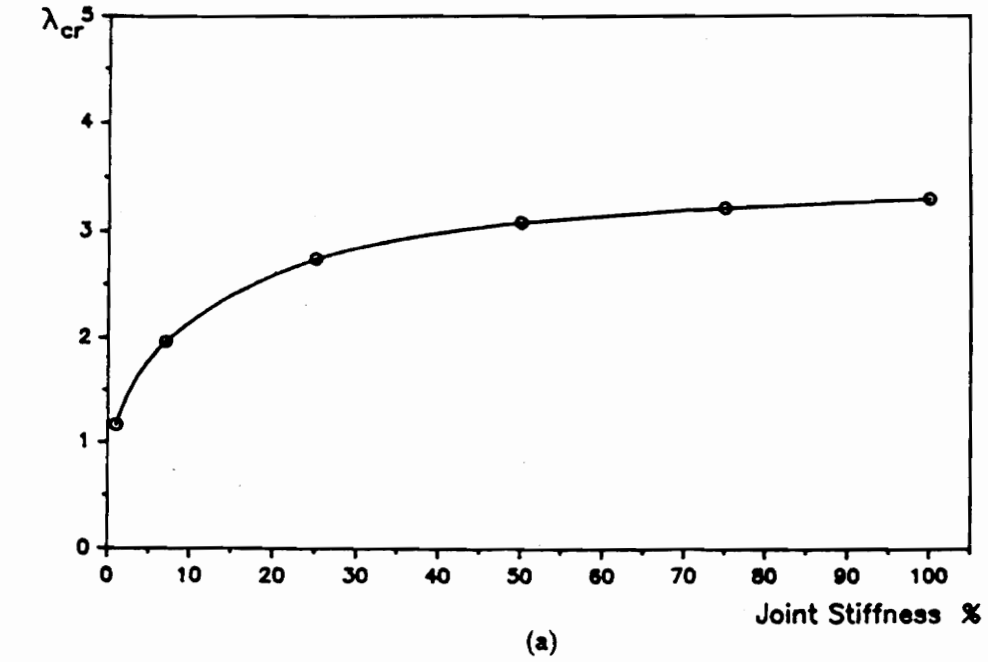

(a)

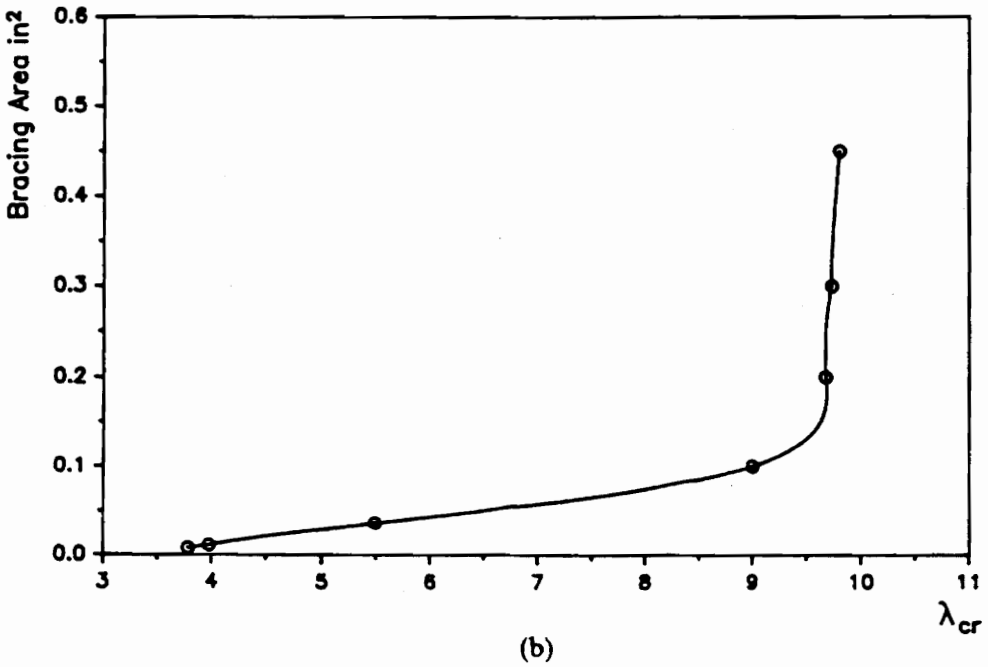

(b)

Figure 6.6. (a) Critical load parameter versus joint stiffness; (b) Bracing area versus critical load parameter.

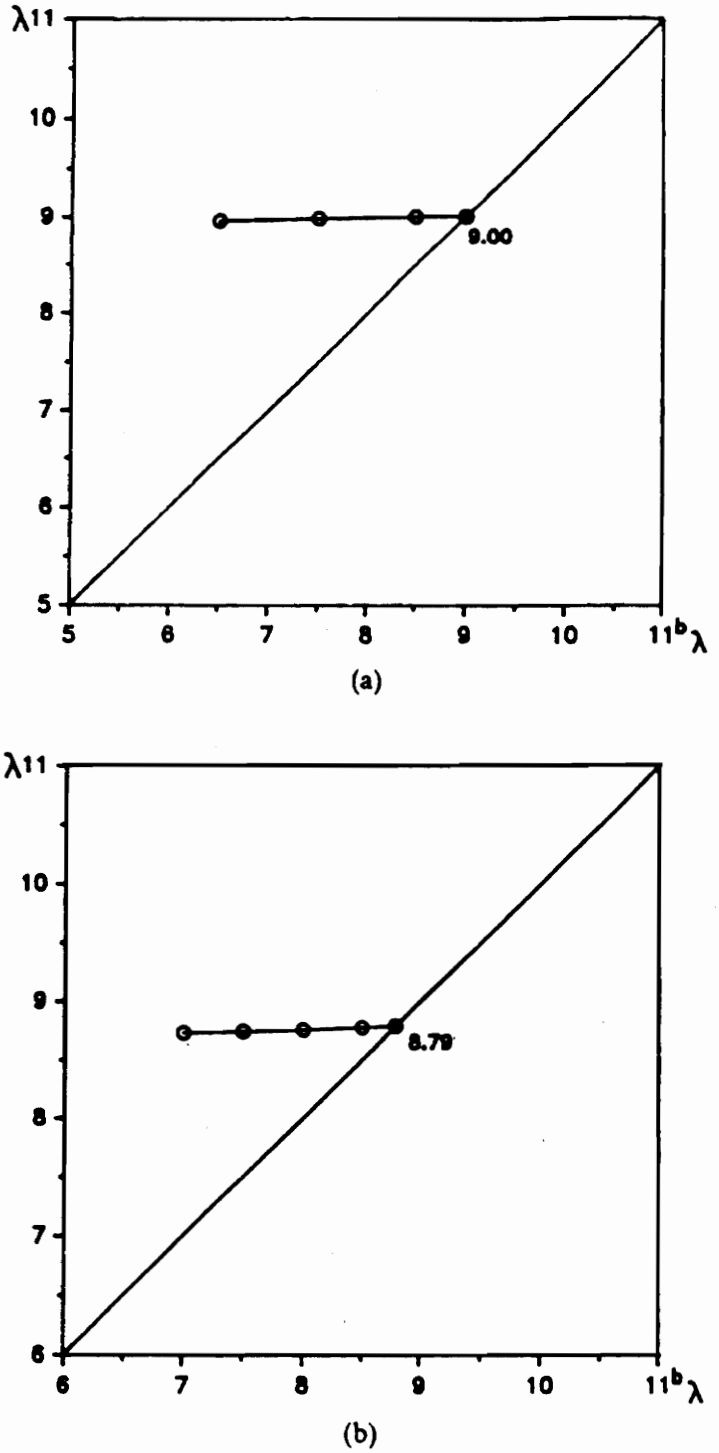

Figure 6.7. Critical load prediction curves of the models with bracing and with (a)100%; (b)25% joint stiffnesses for uniform snow load.

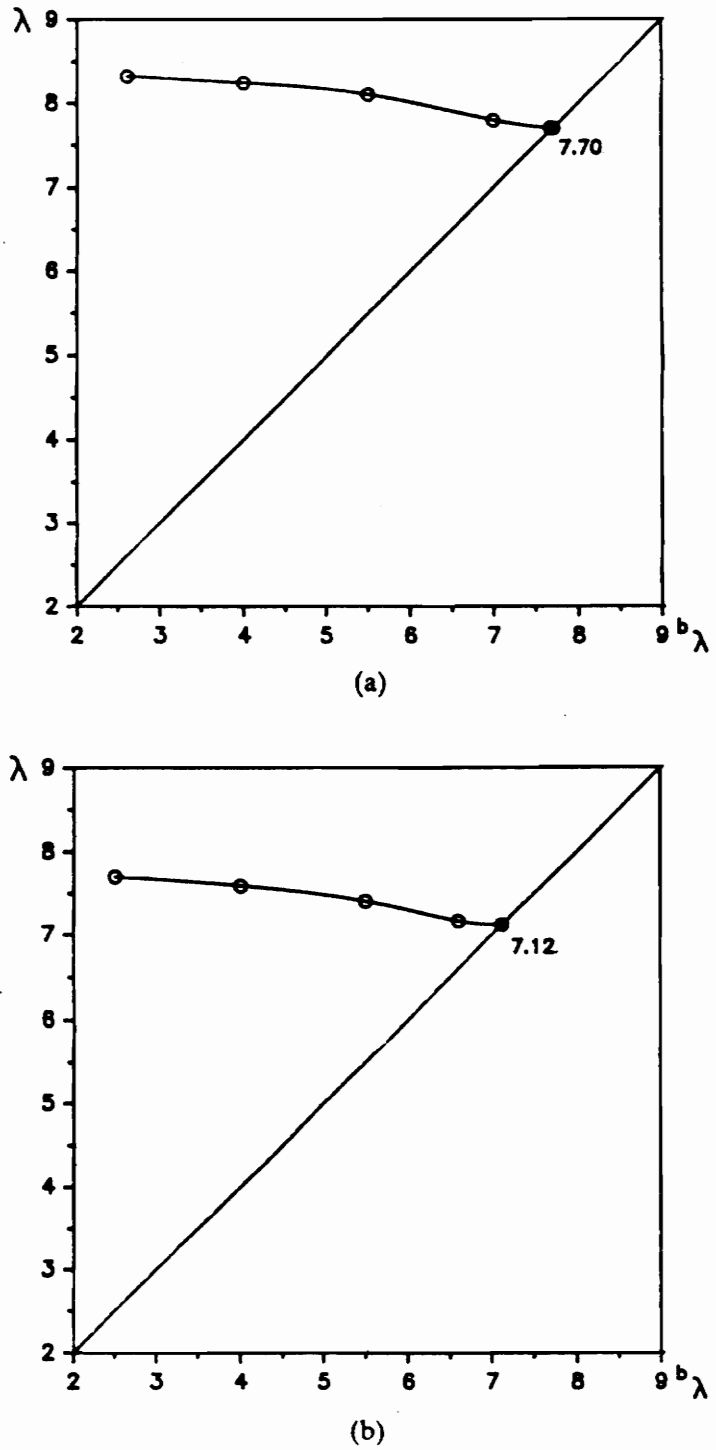

Figure 6.8. Critical load prediction curves of the models with bracing and with (a)100%; (b)25% joint stiffnesses for half snow load.

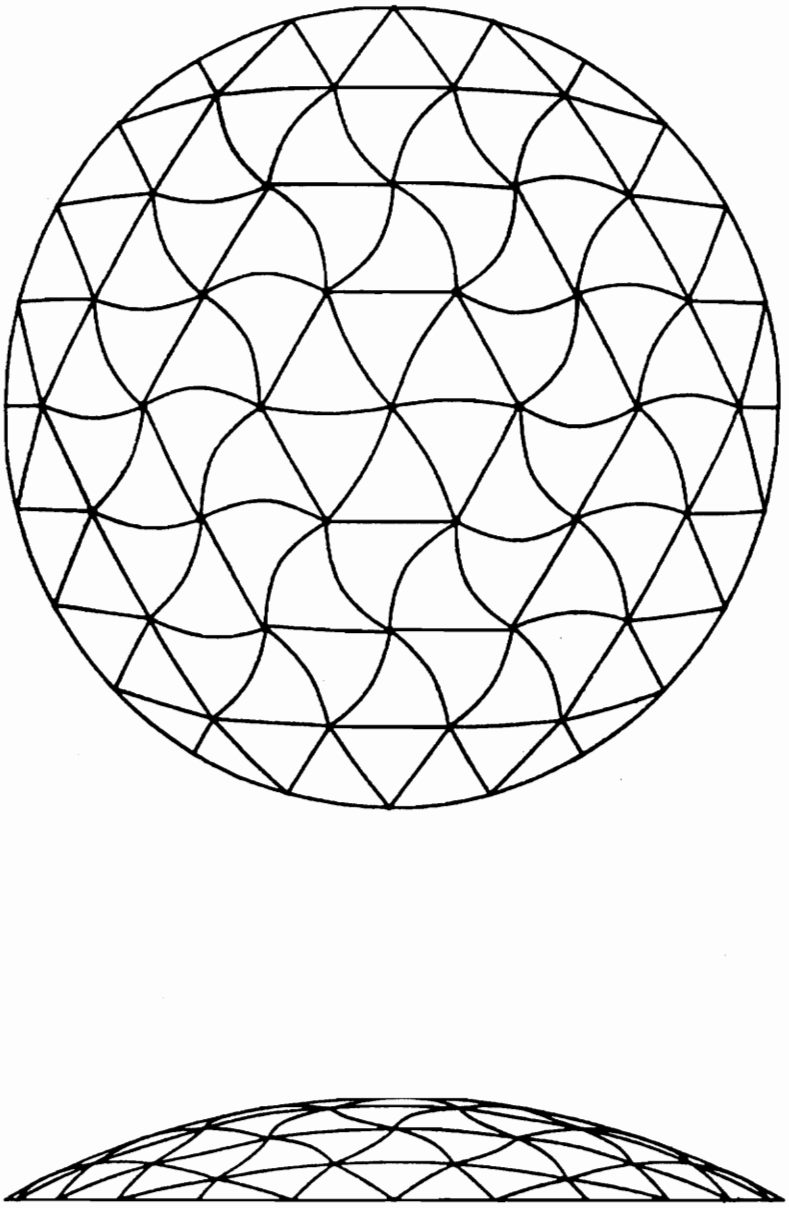

Figure 6.9. Buckling mode of the models with bracing (A = 0.1) and with 100% or 25% joint stiffness for snow over the entire dome.

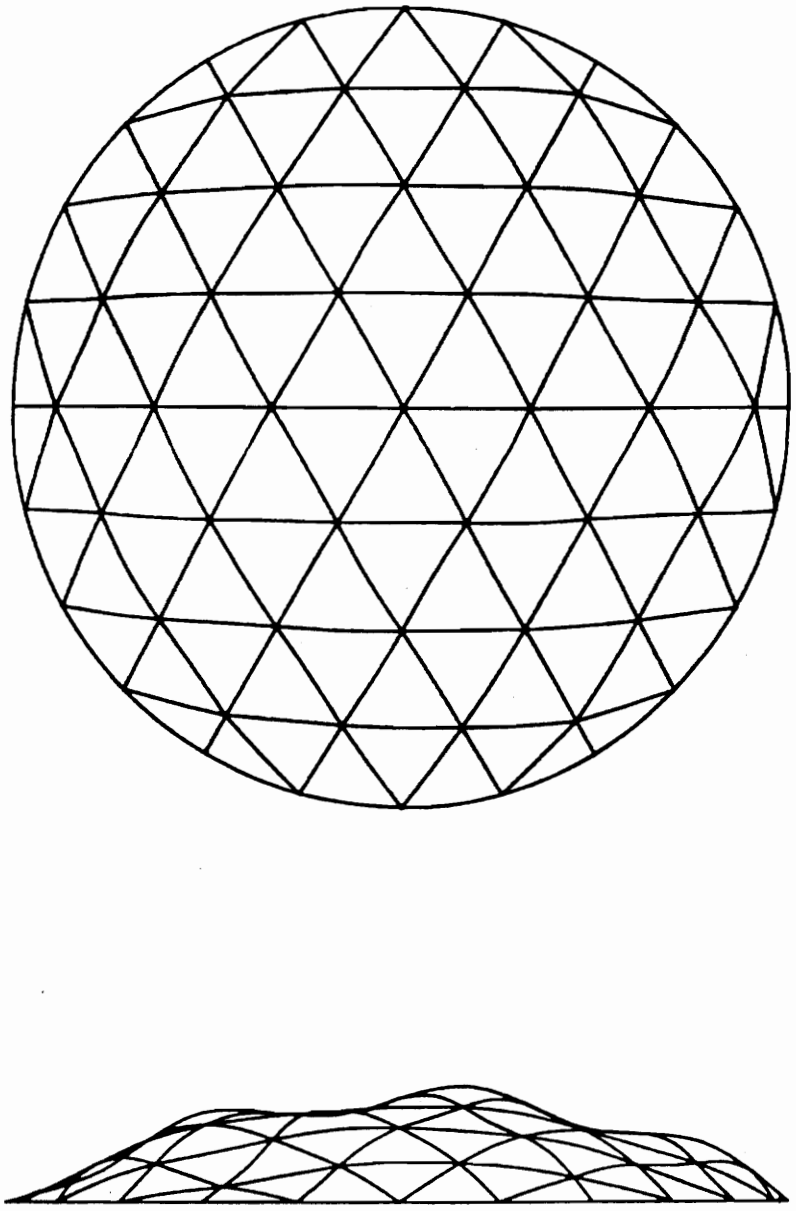

Figure 6.10. Buckling mode of the model with bracing (A = 0.45) and rigid joints for snow over the entire dome.

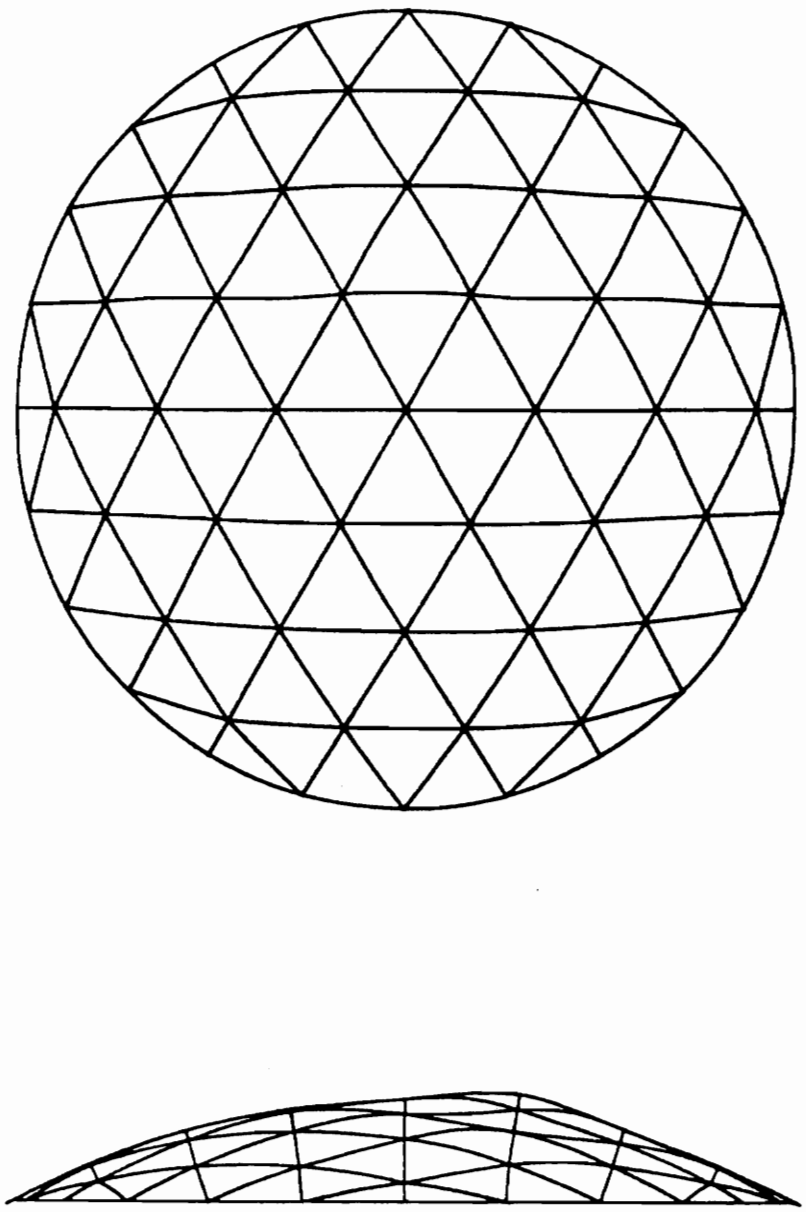

Figure 6.11. Buckling mode of the models with bracing (A = 0.3) and with 100% or 25% joint stiffness for snow over half the dome.

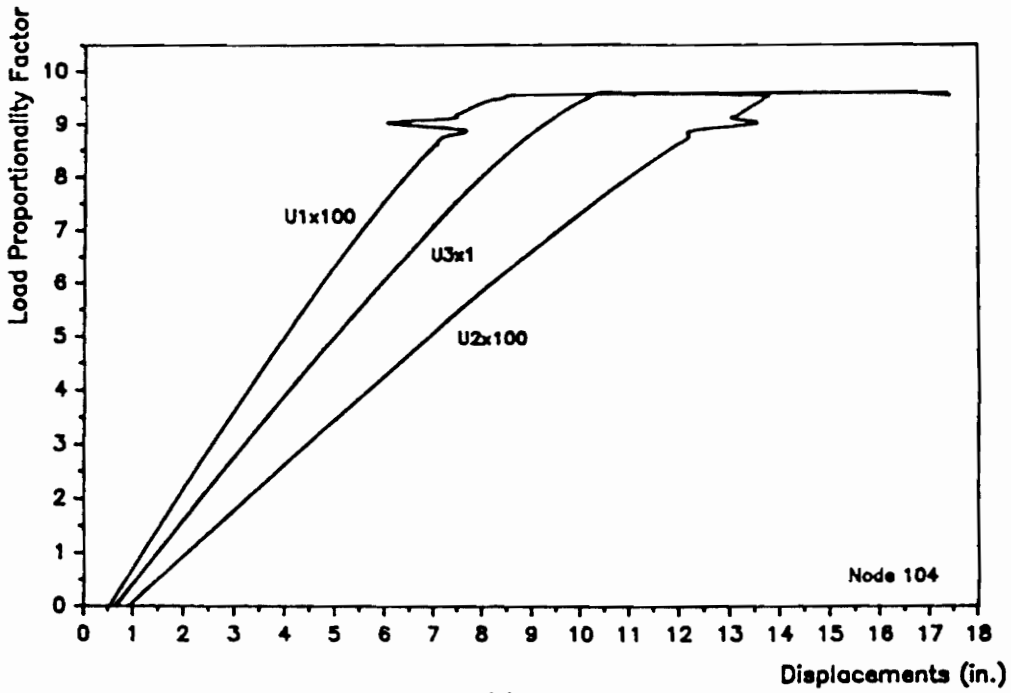

(a)

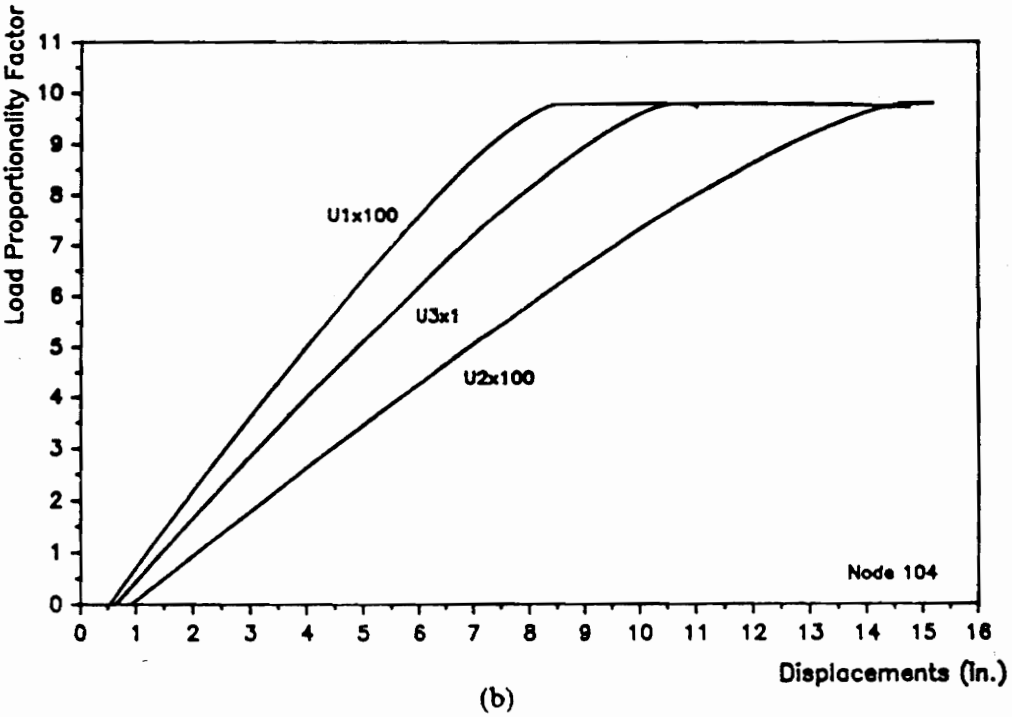

(b)

Figure 6.12. Equilibrium paths of the models with rigid joints and with bracings (a) A = 0.10; (b) A = 0.45 for snow over the entire dome.

Table 6.1(a) Maximum stresses of linear analyses for snow over the entire dome (unit:psi)

Model	Joint Stiffness	Max. Compression of Beams	Max. Tension of Beams	Max. Compression of Purlins	Max. Tension of Purlins	Max. Tension of Steel Bars	Deflection at Apex (Z-Dir.)
Without Bracing	rigid	-1535.0	1229.0	-322.9	63.0	11045.	-1.51
Without Bracing	75 %	-1550.0	1237.0	-322.3	62.9	11047.	-1.51
Without Bracing	50 %	-1587.0	1252.0	-321.2	63.0	11055.	-1.53
Without Bracing	25 %	-1658.0	1298.0	-317.6	63.0	11063.	-1.54
Without Bracing	7 %	-1932.0	1534.0	-305.8	63.8	11091.	-1.61
Without Bracing	1 %	-2375.0	1920.0	-283.7	64.5	11263.	-1.72
With Bracing A = 0.1	rigid	-1417.0	808.2	-323.1	36.9	10632.	-1.48
With Bracing A = 0.1	25 %	-1251.0	781.1	-317.8	38.5	10649.	-1.52

Table 6.1(b) Maximum stresses of linear analyses for snow over half the dome (unit:psi)

Model	Joint Stiffness	Max. Compression of Beams	Max. Tension of Beams	Max. Compression of Purlins	Max. Tension of Purlins	Max. Tension of Steel Bars	Deflection at Apex (Z-Dir.)
Without Bracing	rigid	-1639.0	1159.0	-242.6	56.9	10085.	-1.09
Without Bracing	25 %	-1731.0	1224.0	-237.2	58.9	10096.	-1.12
With Bracing A = 0.3	rigid	-1246.0	1049.0	-257.2	33.7	9341.0	-1.05
With Bracing A = 0.3	25 %	-1115.0	1064.0	-249.4	34.6	9352.0	-1.08

Table 6.2(a) λ_{cr} for snow over the entire dome : $p_{cr} = p_D + \lambda_{cr} p_L$

Joint Stiffness	λ_{cr} Without Bracing	λ_{cr} With Bracing(A=0.1)
rigid	3.30	9.00
75 %	3.22	——
50 %	3.08	8.94
25 %	2.74	8.79
7 %	1.96	——
1 %	1.16	——

Table 6.2(b) λ_{cr} for snow over half the dome : $p_{cr} = p_D + \lambda_{cr} p_L$

Joint Stiffness	λ_{cr} Without Bracing	λ_{cr} With Bracing(A=0.3)
rigid	5.51	7.70
50 %	5.12	7.42
25 %	4.58	7.12

Table 6.3(a) Maximum stresses just before buckling for snow over the entire dome (unit:psi)

Model	Joint Stiffness	Max. Compression of Beams	Max. Tension of Beams	Max. Compression of Purlins	Max. Tension of Purlins	Max. Tension of Steel Bars
Without Bracing	rigid	-4128. A = -685.9 B1=-1406.4 B2=-2035.6	2841. A = -272.6 B1=-1486.9 B2=-1626.6	-749.6	131.0	25185.
Without Bracing	25 %	-3793. A = -590.9 B1=-1345.4 B2=-2036.7	2820. A = -364.7 B1=-1188.2 B2=-1996.3	-632.4	113.7	21738.
With Bracing A = 0.1	rigid	-9798. A =-4181.3 B1=-5609.3 B2= 7.8	4336. A =-1129.5 B1=-3871.5 B2=-1594.0	-1994.	111.2	60223.
With Bracing A = 0.1	50 %	-9748. A =-4201.8 B1=-5536.3 B2= 10.3	4299. A =-1270.5 B1=-4052.5 B2=-1517.0	-1993.	112.6	60671.
With Bracing A = 0.1	25 %	-9764. A =-4183.5 B1=-5576.5 B2= 4.0	4227. A =-1373.0 B1=-4138.5 B2=-1461.5	-1957.	114.4	60596.
With Bracing A = 0.45	rigid	-11399. A =-4567.5 B1=-6831.0 B2= -0.5	4004. A =-1408.8 B1=-4983.3 B2= -429.3	-2291.	——	64967.

Table 6.3(b) Maximum stresses just before buckling for snow over half the dome (unit:psi)

Model	Joint Stiffness	Max. Compression of Beams	Max. Tension of Beams	Max. Compression of Purlins	Max. Tension of Purlins	Max. Tension of Steel Bars
Without Bracing	rigid	-16890. A =-1781.3 B1=-1284.8 B2=13823.8	13327. A =-1781.3 B1=-1284.8 B2=13823.8	-1174.	249.2	34225.
Without Bracing	50 %	-17009. A =-1653.5 B1=-1326.0 B2=14029.5	13702. A =-1653.5 B1=-1326.0 B2=14029.5	-1177.	229.5	32307.
Without Bracing	25 %	-16068. A =-1437.0 B1=-1337.5 B2=13293.5	13194. A =-1437.0 B1=-1337.5 B2=13293.5	-1199.	181.4	29154.
With Bracing A = 0.3	rigid	-17770. A =-4590.0 B1=12153.5 B2= 1026.5	8590. A =-4590.0 B1=12153.5 B2= 1026.5	-1299.	259.5	42629.
With Bracing A = 0.3	50 %	-17825. A =-4426.8 B1=12293.3 B2= 1104.8	8971. A =-4426.8 B1=12293.3 B2= 1104.8	-1188.	309.0	41202.
With Bracing A = 0.3	25 %	-18308. A =-4252.5 B1=12334.5 B2= 1721.0	9803. A =-4252.5 B1=12334.5 B2= 1721.0	-1081.	350.1	39664.

Chapter 7

CONCLUSIONS AND RECOMMENDATIONS

Investigating the stability of a glulam dome with flexible joints and bracings is the principal purpose in this study.

The analyses began with a B32 model, which is a space frame, for four load conditions. The buckling pressure and the buckling mode were determined, and the material behavior prior to buckling was checked. The results are applied as a basis for the analyses of the B33 models.

In the B33 models, purlins are modeled as truss elements. The flexible joints are modeled by specifying a percentage of the moments of inertia of the beam to the connector elements. The contribution of the decking is simulated by the bracing to provide lateral support for the beams.

The effects of the joint stiffness and the bracing on the stability of the dome were discussed. Some conclusions can be made and several recommendations for future studies are presented.

7.1 Conclusions

1. The pre/post processing module contained in I-DEAS is best suited for generating the geometries and the nodal forces, especially for wind load, for the dome model.

2. The B33 beam element can be used to construct the dome model. But more studies on the effect of neglecting the shear deformation are required.

3. For cyclically symmetric load conditions like snow over the entire dome, the critical load prediction curve is nearly a straight horizontal line. The initial critical load prediction (at ${}^{b}\lambda = 0$) is close to the actual critical load. The assumption of the linear buckling theory is realistic.

4. For load conditions like snow over half the dome, the critical load prediction curve is a curve, the initial point tends to underestimate or overestimate the ultimate load.

5. Considering the contribution of the decking, the value of ${}^{b}\lambda$ should be close to the critical load, since the solution of the eigenvalue problem does not converge well for a small value of ${}^{b}\lambda$.

6. The effect of variations in joint stiffness on the stability of the dome is not remarkable:

   a. Neglecting the contribution of the decking, the variations in joint stiffness have the same effect for two load conditions of uniform snow load and half snow load.

   b. Considering the contribution of the decking, the value of the critical load parameter is not sensitive to variations in joint stiffness for the load condition of snow over the entire dome.

c. Considering the contribution of the decking, the value of the critical load parameter is somewhat sensitive to variations in joint stiffness for the load condition of snow over half the dome.

7. The failure modes of the B32 models are bifurcation in the form of twist buckling of the beams when the contribution of the decking is neglected.

8. Bracing is an important component of the load-carrying mechanism; it increases the ultimate load dramatically by strengthening the integral action of the dome for the load condition of snow over the entire dome:

   a. For the load condition of snow over the entire dome, the twist buckling of the beams dominates the failure mode of the dome if the area of the bracing is small or equal to zero. If the area of the bracing is large enough, the failure mode is governed by bending about the local 1 axis of some beams and the critical point is at limit point.

   b. For the load condition of snow over half the dome, bending is always a major part of the load-carrying mechanism, even when the contribution of the decking is neglected. The value of the critical load parameter for the model with bracing is about 147% of that for the model without bracing. In contrast with a 295% for the load condition of snow over the entire dome, the bracing can not overcome the high localized stresses introduced by the unsymmetric load over the dome.

9. If the contribution of the decking is neglected, the minimum value of the critical load parameter for the dome is decided by the load condition of uniform snow load. In contrast, the load condition of half snow load provides the lowest value of the critical load parameter for the dome if the contribution of the decking is considered.

10. The maximum compressive and tensile stresses just before buckling are higher than the proportional limit. The assumption of elastic instability must be revised.

11. Material nonlinearity must be incorporated with geometric nonlinearity in the stability analysis to determine the ultimate load capacity and failure modes of the dome under various load conditions.

7.2 Recommendations

1. In order to incorporate material nonlinearity in the geometrically nonlinear analysis, experimental tests are needed to determine the stress-strain relationships, which cover the elastic and inelatic ranges up to collapse.

2. It appears that the maximum parallel to grain stresses for longleaf pine (Wood Handbook, 1987) is not a best basis to evaluate the material behavior of the glulam dome. More experimental tests are required to accurately estimate the proportional limit and the ultimate stresses of the glulam beams.

3. The effects of imperfections or variations in material properties on the behavior of the glulam dome must be studied.

4. An experiment to test and determine the ultimate load capacity and failure mode for a scaled glulam dome model is necessary for the verification of analytical results. It is possible that the contribution of the decking is overestimated.

5. The effects of geometric imperfections, such as support settlement, fabrication and construction errors on the stability of the glulam dome must be studied. They may dominate the critical state of the glulam dome.

BIBLIOGRAPHY

ABAQUS, *General-Purpose Finite Element System* , Hibbitt, Karlsson & Sorensen, Inc., 100 Medway Street, Providence, RI 02906, U.S.A.

American Institute of Timber Construction, *Timber Construction Mannul* , 3rd. ed., John Wiley & Sons, Inc., New York, 1985.

Baker, S., "A Comparison of the Codes of Practice used in Different Countries for the Determination of Wind Loads on Domes" , Analysis, Design and Construction of Braced Domes, Z. S. Makowski, Ed., Nichols Publishing Company, New York, 1984, pp. 315-336.

Bathe, K. J., *Finite Element Procedures in Engineering Analysis* , Prentice-Hall, Englewood Cliffs, NJ, 1982.

Broyles, L. D., "Triax Domes Modeling With I-DEAS 4.1" , M. S. Thesis, Virginia Polytechnic Institute and State University, January 1990.

Chang, S. C., and Chen, J. J., "Effectiveness of Linear Bifurcation Analysis for Predicting the Nonlinear Stability Limits of Structures" , International Journal for Numerical Methods in Engineering, Vol. 23, 1980, pp. 831-846.

Cook, R. D., Malkus, D. S., and Plesha, M. E., *Concepts and Applications of Finite Element Analysis* , 3rd edition, John Wiley & Sons, 1989.

Davalos, J. F., *Geometrically Nonlinear Finite Element Analysis of a Glulam Timber Dome* , Ph. D. Dissertation, Virginia Polytechnic Institute and State University, July 1989.

European Convention for Constructional Steelwork, *Recommendations for Calculating the Effect of Wind on Constructions* , Second Edition, ECCS Technical Committee 12: Wind, 1987.

Hangai, Y., and Ohya, S., "Buckling Behavior of Reticulated Single-Layer Shells from the viewpoint of Rise-to-Span Ratio" , International Symposium on Innovative Applications of Shells and Spatial Forms, 1988, pp. 393-402.

Holzer, S. M., and Loferski, J. R., "Background for Research on Glulam Lattice Domes" , Proceedings of the Sixth Annual Structures Congress, ASCE Structural Division, Orlando, FL, August 1987, pp. 305-318.

Holzer, S. M., Davalos, J. F., and Huang, C. Y., "A Review of Finite Element Stability Investigations of Spatial Wood Structures" , Bulletin of the International Association for Shell and Spatial Structures, to appear

Holzer, S. M., Wu, C. H., and Tissaoui, J., "Finite Element Stability Analysis of a Glulam Dome" , International Journal of Space Structures, to appear

Huang, C. Y., *Geometrically Nonlinear Finite Element Analysis of a Lattice Dome* , M. S. Thesis, Virginia Polytechnic Institute and State University, November 1989.

I-DEAS, *Engineering Analysis, Model Solution, and Optimization* , Macneal-Schwendler, Structural Dynamics Research Corporation, 2000 Eastman Drive, Milford, Ohio, U.S.A.

Maher, F. J., "Wind Loads on Dome-Cylinder and Dome-Cone Shapes" , Journal of the Structural Division, ASCE, Vol. 92, No. ST5, October 1966, pp. 79-96.

Minimum Design Loads for Buildings and Other Structures, ANSI A58.1-1982, American National Standards Institute, Inc., 1430 Broadway, NY, 10018, 1982.

Neal, D. W., *The Triax Dome* , Culbertson, Noren, and Neal, Consulting Engineers, 1410 S. W. Morrison St., Portland, OR 97205, March 1973.

Newberry, C. W., and Eaton, K. J., *Wind Loading Handbook* , Building Research Establishment Report HM Stationery Office, London, 1974.

Rothert, H., Dickel, T., and Renner, D., "Snap-Through Buckling of Reticulated Space Trusses" , Journal of the Structural Division, ASCE, Vol.107, No. ST1, January 1981, pp. 129-143.

Tacoma Dome, *Pacific Builder and Engineer* , February 7, 1983.

Task Committee on Latticed Structures of the Committee on Metals of the Structural Division, "Lattice Structures : State-of-the-Art Report" , Journal of the Structural Division, ASCE, Vol. 102, No. ST11, Nov. 1976, pp. 2197-2230.

Tsuboi, Y., et al., "Analysis, Design and Realization of Space Frames" , A State-of-the-Art Report by the IASS Working Group on Spatial Steel Structures, Bulletin of the IASS, Vol. XXV-1/2, April-August 1984.

United States Department of Agriculture, *Wood Handbook: Wood as an engineering material, U.S. Forest Products Laboratory* , Agriculture Handbook No. 72, U.S. Government Printing Office, Washington, D.C., 1987.

Appendix A

```
C*****************************************************************
C THE PROGRAM COMPUTES THE COORDINATES OF ADDITIONAL NODES
C FOR CONNECTOR ELEMENTS.
C EACH BEAM CONSISTS OF TWO ELEMENTS.  TWO ADDITIONAL
C NODES NEAR EACH END OF THE BEAM ARE REQUESTED.
C*****************************************************************
C A DATA FILE (UNIT=55), WHICH CONTAINS ALL EXISTING NODAL
C COORDINATES, CAN BE OBTAINED FROM OLD INPUT FILE.
C*****************************************************************
C THE USER MUST PREPARE A DATA FILE (UNIT=60) WITH THREE
C NODES, THE LEFT POINT (N1), THE MID POINT (N2), AND
C THE RIGHT POINT (N3), FOR EACH BEAM.  THE PROGRAM WILL
C COMPUTE THE COORDINATE OF N4, WHICH IS NEAR N1, AND THE
C COORDINATE OF N5, WHICH IS NEAR N3, FOR EACH BEAM.
C*****************************************************************
C  ** VARIABLES: **
C  N,NE= ITERATION COUNTER
C   R  = RADIUS OF CURVATURE OF THE DOME
C   H  = R - RISE OF THE DOME
C   G  = LENGTH OF CONNECTOR ELEMENTS
C   NN = NUMBER OF EXISTING NODES
C   NB = NUMBER OF BEAMS WITH CONNECTOR ELEMENTS
C*****************************************************************
      PARAMETER (NN=217, NB=132)
      DOUBLE PRECISION W1,W2,H1,H2,XA,YA,XB,YB,X1,Y1,Z1,
     $ X2,Y2,Z2,XP3,YP3,S,XC1,YC1,ZC1,XC2,YC2,ZC2,
     $ XC3,YC3,ZC3,AMP1,AMP2,AMP3,UU,UUU,UU1,UU2,UU3,
     $ XP1,YP1,XP2,YP2,U1,U2,U3,B1,B2,B3,V1,V2,R,H,
     $ Q,T,V,G,X(1500),Y(1500),Z(1500)
      OPEN(UNIT=55,STATUS='OLD')
      OPEN(UNIT=60,STATUS='OLD')
      OPEN(UNIT=90,STATUS='UNKNOWN')
      R=1600.
      H=1387.66
      G=5.5
      N6= 0
CC ***************  READ EXISTING NODES
      DO 10 I=1,NN
         READ (55,*) N, Q, T, V
         X(I) = Q
         Y(I) = T
         Z(I) = V+H
10    CONTINUE
CC ***************  CAL. ADDITIONAL NODES' COORDINATES
      DO 60 J=1,NB
         READ (60,*) NE, N1, N2, N3
         XC1 =  X(N1)
         YC1 =  Y(N1)
         ZC1 =  Z(N1)
         XC2 =  X(N3)
         YC2 =  Y(N3)
         ZC2 =  Z(N3)
```

```
            XC3 =  X(N2)
            YC3 =  Y(N2)
            ZC3 =  Z(N2)
            AMP1=ZC1/H
            AMP2=ZC2/H
            AMP3=ZC3/H
            XP1=XC1/AMP1
            YP1=YC1/AMP1
            XP2=XC2/AMP2
            YP2=YC2/AMP2
            XP3=XC3/AMP3
            YP3=YC3/AMP3
C
            U1=DSQRT(XP1**2+YP1**2+H**2)
            U2=DSQRT(XP2**2+YP2**2+H**2)
            U3=DSQRT(XP3**2+YP3**2+H**2)
            B1=DACOS(H/U1)
            B3=DACOS(H/U3)
            UU1=U1*DSIN(B1)
            UU3=U3*DSIN(B3)
            S=G/R
            UU=DSQRT((XP1-XP3)**2+(YP1-YP3)**2)
C
            IF (UU1 .GT. UU) THEN
               GO TO 20
            ENDIF
            IF (UU3 .GT. UU) THEN
               GO TO 20
            ENDIF
            W1=H*DTAN(B1-S)
            GO TO 30
C
20          IF (ZC3 .GT. ZC1) THEN
               W1=H*DTAN(B1-S)
            ELSE
               W1=H*DTAN(B1+S)
            ENDIF
C
30          H1=DABS(UU1-W1)
            XA=XP1-(XP1-XP3)*H1/UU
            YA=YP1-(YP1-YP3)*H1/UU
            V1=DSQRT(XA**2+YA**2+H**2)
            X1=XA*R/V1
            Y1=YA*R/V1
            Z1=H*R/V1-H
C
            B2=DACOS(H/U2)
            UU2=U2*DSIN(B2)
            UUU=DSQRT((XP2-XP3)**2+(YP2-YP3)**2)
            IF (UU2 .GT. UUU) THEN
               GO TO 40
            ENDIF
            IF (UU3 .GT. UUU) THEN
               GO TO 40
```

```
            ENDIF
            W2=H*DTAN(B2-S)
            GO TO 50
C
40             IF (ZC3 .GT. ZC2) THEN
                  W2=H*DTAN(B2-S)
               ELSE
                  W2=H*DTAN(B2+S)
               ENDIF
C
50          H2=DABS(UU2-W2)
            XB=XP2-(XP2-XP3)*H2/UUU
            YB=YP2-(YP2-YP3)*H2/UUU
            V2=DSQRT(XB**2+YB**2+H**2)
            X2=XB*R/V2
            Y2=YB*R/V2
            Z2=H*R/V2-H
C
            N4=N6*2+1
            N4=N4+NN
            N5=N4+1
            N6=N6+1
            WRITE (90,250) N4,X1,Y1,Z1
            WRITE (90,250) N5,X2,Y2,Z2
C
60       CONTINUE
250      FORMAT (7X,I4,',',E15.7,',',E15.7,',',E15.7)
         END
```

Appendix B

COMPARISON OF ELEMENT STRESSES FOR THREE B33 MODELS

Element Number	B33 Model Without Connector Element Purlin Acts As Beam		B33 Model With Connector Elements Purlin Acts As Beam		B33 Model With Connector Elements Purlin-Truss Element	
290	-602.4	-461.7	-590.0	-448.2	-591.1	-450.0
289	-526.1	-642.6	-518.0	-642.0	-515.3	-656.6
288	-879.3 266.2	-1018.0 406.9	-826.1 208.4	-1011.0 395.9	-822.2 206.9	-1016.0 403.2
298	-662.3	-810.3	-649.2	-797.9	-605.3	-798.1
297	-693.2	-665.3	-678.3	-661.9	-692.1	-685.1
311	-1354.0	-771.7	-1315.0	-775.5	-1323.0	-805.5
312	-736.3	-760.2	-736.9	-752.2	-725.3	-771.9
335	-975.4	-1560.0 119.4	-980.4	-1478.0 33.9	-973.4	-1466.0 20.5
336	-820.1	-992.8	-815.3	-985.8	-819.0	-978.8
302	-769.6	-713.9	-757.1	-705.7	-776.1	-711.9
301	-726.4	-661.3	-718.0	-681.7	-724.0	-678.2
296	-1461.0 829.0	-1540.0 910.2	-1358.0 721.1	-1534.0 899.8	-1354.0 715.9	-1535.0 899.8
295	-1537.0 916.4	-1517.0 894.5	-1531.0 906.0	-1413.0 785.5	-1532.0 906.1	-1414.0 785.7
320	-658.5	-695.0	-647.9	-689.9	-650.3	-693.2
319	-705.7	-604.1	-701.0	-605.0	-706.6	-593.3
317	-700.7	-700.2	-696.9	-696.2	-692.5	-699.8
318	-745.0	-714.1	-739.9	-708.2	-748.4	-704.6
310	-1005.0 797.6	-1427.0 1221.0	-894.5 682.3	-1428.0 1218.0	-880.9 666.4	-1427.0 1215.0
309	-1429.0 1236.0	-1382.0 1186.0	-1429.0 1232.0	-1254.0 1054.0	-1429.0 1228.0	-1269.0 1066.0
308	-1467.0 1159.0	-1491.0 1187.0	-1339.0 1025.0	-1490.0 1178.0	-1335.0 1023.0	-1494.0 1185.0

COMPARISON OF ELEMENT STRESSES FOR THREE B33 MODELS

334	-337.5 172.9	-573.1 370.1	-341.1 137.1	-578.7 376.2	-360.5 149.7	-575.5 365.9
333	-538.8 290.8	-462.8 213.7	-537.4 289.6	-441.5 192.7	-588.5 335.3	-474.3 219.7
331	-877.9	-978.0	-891.4	-958.8	-845.1	-986.0
332	-783.8	-921.4	-748.2	-918.9	-777.4	-857.7
330	-503.3	-610.2	-506.4	-622.1	-480.2	-661.9
329	-671.5	-546.1	-669.9	-580.9	-673.0	-590.8
349	-384.2	-384.3	-381.1	-381.3	-322.9	
350	-298.2	-298.3	-293.7	-293.9	-233.8	
351	-302.3	-303.5	-298.9	-300.1	-258.6	
355	-252.8	-253.3	-250.2	-250.7	-206.7	
356	-276.0	-198.3	-271.1	-196.9	-186.3	
357	-263.4	-269.2	-264.8	-267.7	-228.1	
360	-111.5	111.5	108.3	108.3	63.0	
361	-116.1 185.5	-135.4 205.3	-111.3 181.0	-137.5 207.7	33.8	
362	-263.8 360.1	-191.2 286.8	-252.9 349.8	-193.3 289.6	47.7	
344	-779.9 978.3	-655.0 855.2	-780.6 978.9	-653.1 853.2	-781.8 979.2	-648.7 847.9
343	-661.1 861.3	-741.5 940.0	-659.5 859.6	-740.0 938.5	-655.2 854.4	-739.8 937.3
342	-813.2 1047.0	-795.8 1031.0	-822.2 1057.0	-796.2 1033.0	-840.4 1076.0	-800.8 1039.0
341	-798.2 1034.0	-712.1 945.8	-798.8 1035.0	-710.3 944.9	-803.2 1041.0	-710.7 946.6
348	10726.0		10744.0		10761.0	
347	11026.0		11045.0		11045.0	

Note: 1. Stresses at two ends are listed for each element.
2. A negative value of stress means Compression.
A positive value of stress means tension.
3. The stresses of connector elements are not listed.
4. Refer to Fig. 3.5(b) for elements number.

Vita

Chen-Hung Wu was born in Tainan, Taiwan. He graduated from National Chen Kung University with a Bachelor of Science degree in Civil Engineering in June 1973. After fulfilling military service for two years, he began to work as a civil engineer. He came to Virginia Polytechnic Institute and State University in August 1989 for his graduate education. Studying in Blacksburg is a joyful experience for him. He tried to learn as much as he could. He is now completing his graduate studies for a Master of Science degree and is expecting to continue his engineer career in his home country.